THIN-FILM $Pb_{0.9}Sn_{0.1}Se$ PHOTOCONDUCTIVE INFRARED DETECTORS: PHOTOCONDUCTIVITY MEASUREMENTS

Kurt Ervin Holmquist

NAVAL POSTGRADUATE SCHOOL
Monterey, California

THESIS

THIN-FILM $Pb_{0.9}Sn_{0.1}Se$
PHOTOCONDUCTIVE INFRARED DETECTORS:
PHOTOCONDUCTIVITY MEASUREMENTS

by

Kurt Ervin Holmquist

Thesis Advisor: T.F. Tao

December 1972

Thin-Film $Pb_{0.9}Sn_{0.1}Se$ Photoconductive Infrared Detectors: Photoconductivity Measurements

by

Kurt Ervin Holmquist
Lieutenant, Junior Grade, United States Navy
B.S.E.E., United States Naval Academy, 1971

Submitted in partial fulfillment of the
requirements for the degree of

MASTER OF SCIENCE IN ELECTRICAL ENGINEERING

from the

NAVAL POSTGRADUATE SCHOOL

December 1972

ABSTRACT

$Pb_{0.9}Sn_{0.1}Se$ thin films were deposited on cleaved CaF_2 and BaF_2 substrates by vacuum evaporation methods. The as-deposited films were not photosensitive. Photoconductivity was observed after the films had been isothermally annealed in Pb-Sn rich vapor to reduce their carrier concentrations. Blackbody (500° K) response measurements were made to determine the responsivity and detectivity of the thin-film samples. Blackbody responsivities as high as 60 volts per watt were measured. Thin films with single-crystal (100)-oriented structure were more sensitive than the films with either single-crystal (111) or polycrystalline mixed (111) and (100) structure. The wavelengths of photoconductive thresholds were determined by spectral response measurement and were in good agreement with the fundamental absorption edges. Photoconductive response times were measured using a GaAlAs heterojunction laser diode as the radiation source.

TABLE OF CONTENTS

LIST OF FIGURES

LIST OF TABLES

ACKNOWLEDGEMENT

The author wishes to express his indebtedness and sincere gratitude to Dr. T. F. Tao for his guidance, assistance and encouragement in this work, and to the Office of Naval Research and the Air Force Materials Laboratory for supporting this research.

I. INTRODUCTION

Considerable progress has been made in the past few years in developing long-wavelength infrared (LWIR) devices for imaging, surveillance, and remote sensing applications, and for use in CO_2 laser systems. One of the most important advancements is the development of narrow-gap IV-VI alloy semiconductor devices. Considerable attention has been given to two alloy systems, $Pb_{1-x}Sn_xTe$ and $Pb_{1-y}Sn_ySe$ [Refs. 3 through 10]. Their p-n homojunctions now have adequate device performance when used as practical photovoltaic detectors[1] and as semiconductor lasers.[2]

In comparison, however, photoconductivity in these two alloy systems has not been well developed. Of these two alloys, $Pb_{1-x}Sn_xTe$ photoconductors have been relatively more developed. Photoconductivity in bulk $Pb_{1-x}Sn_xTe$ crystals was first studied at Lincoln Laboratory, Massachusetts Institute of Technology.[3] Subsequently, photoconductivity

---

[1] Melngailis, I. and Harman, T.C., "Single Crystal Lead-Tin Chalcogenides," Semiconductors and Semimetals, v. 5, p. 354-365, March, 1968.

[2] Harman, T.C., "Narrow-Gap Semiconductor Lasers," Journal of Physics and Chemistry of Solids, v. 32, Supplement 1, p. 363, 1971.

[3] Melngailis, I. and Harman, T.C., "Photoconductivity in Single-Crystal $Pb_{1-x}Sn_xTe$," Applied Physics Letters, v. 13, p. 180-183, Sept 1968.

in $Pb_{1-x}Sn_xTe$ thin films was reported by Dr. T. F. Tao and Dr. C. C. Wang[4] and by Ford Scientific Laboratory.[5] The present $Pb_{1-x}Sn_xTe$ photoconductive performances are presented in Table I. Peak responsivities occur in the wavelength range of 8 to 11 microns and are less than 10 volts per watt at liquid nitrogen temperatures.

Although several attempts have been made in developing $Pb_{1-y}Sn_ySe$ photoconductive detectors at RCA Princeton Research Laboratory and at General Electric Research Laboratory, no quantitative results indicating true photoconductivity in $Pb_{1-y}Sn_ySe$ have been reported. Some preliminary study of $Pb_{1-y}Sn_ySe$ has been done by Dr. I. Kasai and Dr. C. C. Wang. The purpose of this thesis project was to develop $Pb_{1-y}Sn_ySe$ photoconductivity more extensively. The composition y = 0.1 was used because its energy gap at liquid nitrogen temperature is suitable for infrared detection in the 8 to 14-micron atmospheric window. This was a joint thesis project conducted by the author and CAPT W.G. McBride, USMC. Both were involved in all aspects of this research, although, in the writing of the thesis reports only, McBride concentrated on the metallurgical and electrical properties and the author of this paper concentrated on the photoconductive properties.

---

[4] Tao, T.F. and Wang, C.C., Narrow-Gap Semiconductors, U.S. Air Force Materials Laboratory Report AFML-TR-71-238 (unpublished), Wright Patterson Air Force Base, December, 1971.

[5] Logothetis, E. M. and Holloway, H., "Photoconductivity in Epitaxial $Pb_{1-x}Sn_xTe$," Journal of Applied Physics, v. 43, p. 256-257, January 1972.

TABLE I

PROPERTIES OF PHOTOCONDUCTIVE $Pb_{1-x}Sn_xTe$ BULK SINGLE CRYSTALS AND THIN FILMS

	POLYCRYSTALLINE (100) FILMS			
	One Boat Evaporation	Flash Evaporation	Single-Crystal (111) Film	Bulk (100) Single-Crystals
Composition (x)	0.14	0.14	0.17	0.17
Thickness (microns)	4.4	5	3	50
Sensitive area (cm^2)	0.2	0.21	0.25	0.08
Carrier concentration (cm^{-3})[a]	3.5×10^{17}(n)	8×10^{16}(p)	3.9×10^{16}(n)	5.8×10^{15}(p)
Mobility (cm^2-v^{-1}-sec^{-1})[a]	3.9×10^3	2×10^2	1.4×10^4	2.6×10^4
Temperature (°K)	100	77	77	77
Resistance (ohm)	50	9000	380	10
Bias (ma)	17	1.5	15	10
Peak wavelength (micron)	8.3	8	8.9[b]	10
Peak responsivity (V/W)	5.2	9.7	13.2[c]	0.7
Peak detectivity (cm-W^{-1}-$Hz^{-\frac{1}{2}}$	1.2×10^9	1.7×10^8	6.6×10^8	3×10^8

a) 87° K b) 84° K c) Multiply by 2.45

II. SUMMARY OF PREPARATION, METALLURGICAL EVALUATION, AND ELECTRICAL MEASUREMENTS OF $Pb_{0.9}Sn_{0.1}Se$ THIN FILMS

The $Pb_{0.9}Sn_{0.1}Se$ studied in this research was in the form of thin films deposited on CaF_2 and BaF_2 substrates using the one-boat deposition method or the Knudson cell deposition method. Metallurgical measurements were then made on the samples in order to determine their crystal structure, orientation, and thickness. Following these, the samples were isothermally annealed in the presence of PbSn-rich vapor to reduce their carrier concentrations. Gold contacts were deposited and copper leads attached. Conventional electrical measurements based on the Hall effect were then made from 300° K to 90° K to determine the carrier type, carrier concentration and Hall mobility. This chapter is a brief summary of the material presented in detail by McBride in his paper [Ref. 1] dealing with the first phases of this research: sample preparation, metallurgical evaluation, isothermal annealing, and electrical measurements.

A. SAMPLE PREPARATION

Stoichiometric proportions of Pb, Sn, and Se were weighed and melted at 1100°C for 24 hours in a vacuum-sealed quartz ampoule. The ampoule was then quenched in water and the $Pb_{0.9}Sn_{0.1}Se$ alloy ingot was crushed into small pieces for use in deposition. Metal-rich alloy of the composition $(Pb_{0.9}Sn_{0.1})_{1.04}Se$ was also prepared in the same manner for

use in the isothermal annealing step. Half-inch diameter rods of CaF_2 and BaF_2 were cleaved along the (111) plane shortly before deposition to make substrates approximately 0.3 cm thick which were then loaded in a substrate holder which was placed in a NRC vacuum system. A mask was used over each substrate so that the shape of the thin film was a standard configuration designed for making Hall effect measurements (Figure 1). A heater element was placed above the substrate holder to control the substrate temperature during the deposition. Several small chunks of the stoichiometric $Pb_{0.9}Sn_{0.1}Se$ source material were placed in a graphite Knudson cell or alumina crucible located approximately six inches beneath the substrate holder. The source boat was surrounded by a tungsten heating coil and covered with a molybdenum sheet having a small hole. A shutter was located between the holder and the boat to control the deposition. Prior to the deposition, the vacuum system was evacuated to the low 10^{-6} torr range and the substrate was heated to the desired temperature (270° C to 325° C). The Knudson cell was heated to the range from 740° C to 820° C. After several minutes, the shutter was opened and the evaporated $Pb_{0.9}Sn_{0.1}Se$ was allowed to condense on the substrate forming a thin film. The depositon typically lasted from fifteen to thirty minutes. After deposition, the system was allowed to cool to room temperature in typically three hours. The samples were then removed, inspected, and stored in a

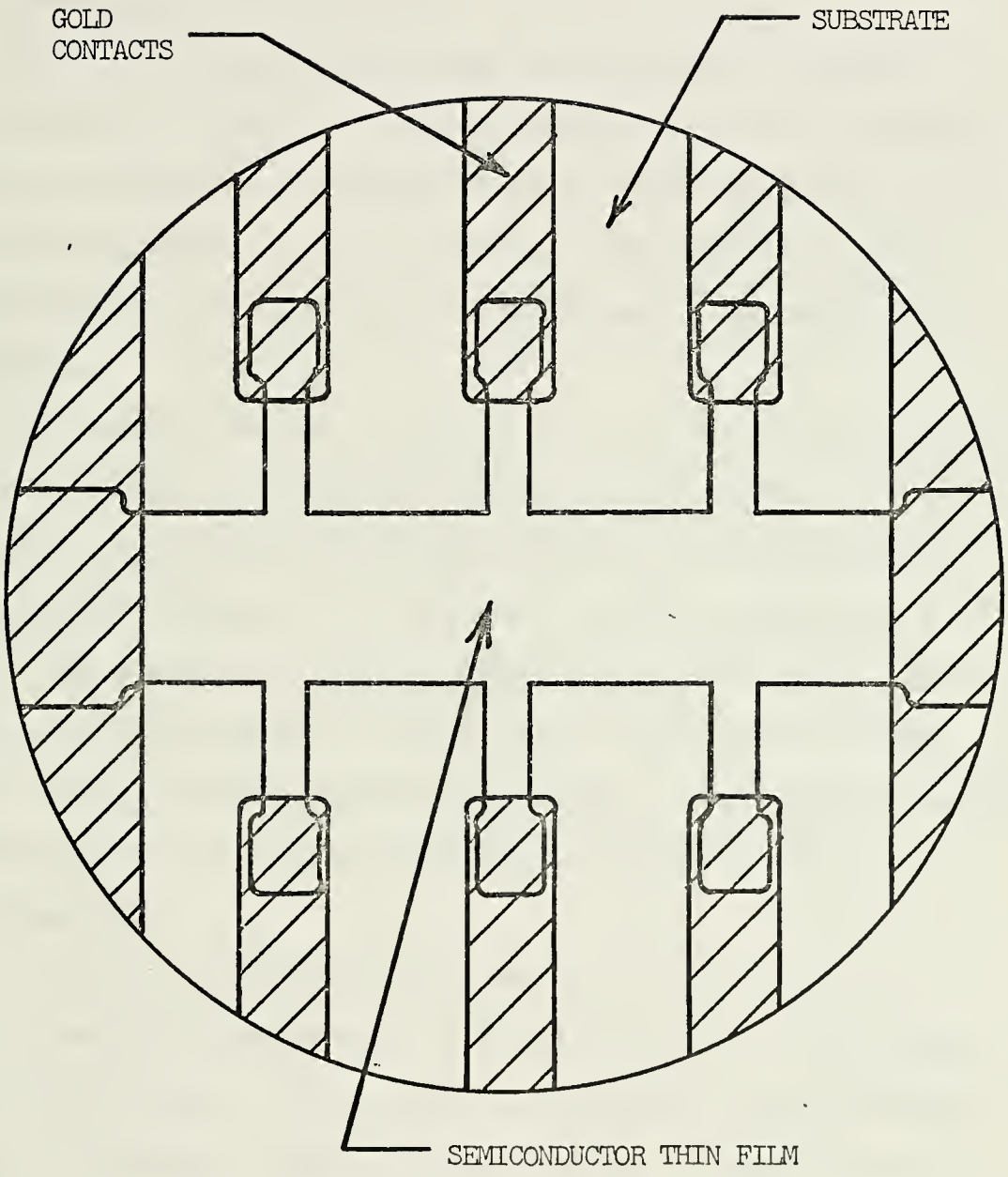

FIGURE 1. DRAWING OF A THIN-FILM SAMPLE

dessicator. Thin films deposited in this manner exhibited good adhesion to the substrate and were generally shiny in appearance.

B. METALLURGICAL EVALUATION

The thickness of each sample was measured using the interferometric method on a Perkin-Elmer spectrophotometer. A scan was obtained of transmittance versus wavelength from 2.5 to 16 microns, and the wavelength difference between the peaks shown in the scan was measured to determine the thickness.

One sample from each deposition batch underwent measurements in order to determine the crystal properties. The crystal structure was evaluated from Laue back-reflection photographs obtained on a Norelco Laue back-reflection X-ray unit. The presence of Debye rings on the photograph indicated polycrystalline structure while sharp spots and no Debye rings indicated single-crystal structure. Both single-crystal and polycrystalline thin-film samples were deposited for this research.

The crystal orientation was determined from X-ray diffractometer scans done on a Norelco X-ray diffractometer using a Cu target. The crystal orientation was determined from the position of the intensity peaks. Single-crystal (100), polycrystalline (100)+(111), as well as polycrystalline (110) films were obtained on CaF_2 substrates, while only single-crystal (111) was obtained on BaF_2.

C. ISOTHERMAL ANNEALING

The carrier concentrations of the as-deposited thin-films were reduced using the isothermal annealing technique which was first used by Brebrick and Allgaier for PbTe [Ref. 2]. Following the metallurgical evaluation, the samples were sealed in quartz annealing ampoules which had been evacuated and back-filled with helium gas. Each tube contained two samples and a small amount of metal-rich source material. These samples were annealed in Marshall tubular ovens the temperature of which was regulated at a set constant value by Marshall proportional controllers. Annealing temperatures from 303° C to 324° C were used for periods of time from two to five days. At the end of the annealing period, the annealing tubes were removed from the ovens and air-cooled to room temperature. The isothermal annealing process reduced the carrier concentrations to a range from middle-10^{16} to middle-10^{17} per cubic centimeter. Annealing temperatures and times were selected based on experience and on the results of other research in this area. $Pb_{0.9}Sn_{0.1}Se$ samples annealed at temperature below 319.5° C were p-type and those annealed at higher temperatures were n-type. Following the annealing, gold contacts were vacuum-deposited on the samples using the NRC vacuum system and copper leads were attached using silver epoxy. A drawing of the shape of the thin-film samples showing the positions of the gold pads is shown in Fig. 1.

D. ELECTRICAL MEASUREMENTS

Electrical measurements were made on the samples to determine the carrier type, concentration, and mobility using the Hall effect technique [Ref. 11]. Samples were mounted on the cold-finger of a liquid-nitrogen dewar. The temperature of the sample was monitored using a thermocouple mounted on a blank substrate on the other side of the cold-finger. The dewar was evacuated to twenty microns Hg or less and cooled to 90° K. The conductivity versus temperature was determined during the cooling process by ploting the voltage across a pair of contacts parallel to the current flow on the horizontal input of an x-y recorder. The current through the sample was kept constant at one milliampere and the thermocouple was connected to the vertical input of the recorder. The Hall voltage was measured across a pair of contacts perpendicular to the bias current flow when a 5000 Gauss magnetic field was passed through the sample perpendicular to the plane of the thin film. The Hall voltage versus temperature was obtained by plotting this voltage on the recorder as the magnetic field was alternately turned on and off and as the temperature of the sample was gradually brought up to room temperature. Calculations were made from these two plots of the Hall coefficient, conductivity, mobility, and carrier type and concentration. Mobilities were measured in the range from 80 to 29,000 cm^2-$volt^{-1}$-sec^{-1} and carrier concentrations of both p-type and n-type were measured from middle-10^{16} to middle-10^{17} cm^{-3}.

III. GENERAL THEORY OF PHOTOCONDUCTIVITY AND INFRARED PHOTODETECTOR PERFORMANCE MEASUREMENT

A. PHOTOCONDUCTIVITY

1. Definition of Photoconductivity

Photoconductivity is defined simply as a change in the electrical conductivity of a material caused by incident light energy. When a photoconducting material is exposed to electromagnetic radiation, a flux of photons proportional to the intensity of radiation will penetrate the material. If the quantum energy of a photon is greater than the forbidden energy gap for electrons in the material, an electron in the valence band may absorb this energy and be excited into the conduction band. This electron in the conduction band and the hole left behind in the valence band are now both free to move under the force of an externally applied electric field and thereby contribute to the electric current. This change in the number of free carriers appears as a change in the electrical conductivity of the material as shown in the following relations.

$$\sigma_o = e(n_o\mu_e + p_o\mu_h)$$

$$\Delta\sigma = e(\Delta n\mu_e + \Delta p\mu_h)$$

Here, σ_o, n_o, p_o are the dark conductivity, free electron, and free hole concentrations caused by thermal excitation, and

$\Delta\sigma$, Δn, and Δp are the changes in these quantities due to incident light; μ_e and μ_h are the electron and hole drift mobilities, and e is the electronic charge. If a constant bias current flows through a photoconductor, the incidence of electromagnetic radiation will be detected as a change in the voltage across the device. Equivalently, if the bias is a constant voltage, incident radiation will cause a change in the current through the sample.

2. Excess Carrier Lifetime and Photoconductive Gain

The magnitude of the response of a photoconductor to a given intensity of radiation and with a given bias condition depends entirely on the density of photo-excited free carriers. In an intrinsic photo-conductor, since free electrons and free holes are generated at the same rate, this density can be approximated by the product of the rate of generation of free electron-hole pairs per unit volume (f) and the excess carrier lifetimes (τ_e and τ_h). In more careful analysis, the radiation intensity inside the sample is not a constant and differential equations must be solved.

$$\Delta n = f\tau_e \qquad \Delta p = f\tau_h$$

The excess carrier lifetime is defined from the microscopic point of view as the average time spent by a photo-generated excess carrier in its respective band and from the macroscopic point of view as the ratio of the density of free carriers to the rate of generation per unit volume. Substitution of

the above expressions for excess free carrier densities into the equation for the change in conductivity gives the following relation.

$$\Delta\sigma = ef(\tau_e\mu_e + \tau_h\mu_h)$$

The significance of lifetime is most apparent in the expression for the gain of a photoconductor. The current is a photoconductor due to incident light energy is the total excess electric charge (n_t and p_t) divided by the transit time of a charge carrier from one electrode to the other ($T_{\tau e}$ and $T_{\tau h}$).

$$I_{ph} = e\frac{n_t}{T_{\tau e}} + e\frac{p_t}{T_{\tau h}}$$

Representing the total rate of generation of electron-hole pairs as F and writing the transit time in terms of the spacing between electrodes (L), the mobility (μ), and the applied voltage (V), gives the following expressions:

$$n_t = F\,\tau_e \qquad p_t = F\,\tau_h$$

$$T_\tau = \frac{L}{\nu} = \frac{L}{\mu\varepsilon} = \frac{L^2}{\mu V}$$

In the second expression, ν is the carrier drift velocity and ε is the electric field strength. Substitution of these into the equation for the photo-current leads to the expression

for photoconductive gain. The gain is essentially the number of excess carriers which pass between the electrodes for each incident photon.

$$I_{ph} = eF\left(\frac{\tau_e}{T_{\tau_e}} + \frac{\tau_h}{T_{\tau_h}}\right)$$

$$I_{ph} = eF \frac{V}{L^2} (\tau_e \mu_e + \tau_h \mu_h)$$

$$b = \mu_e / \mu_h$$

$$I_{ph} = \frac{eF\mu_h V}{L^2} (b\tau_e + \tau_h)$$

$$G = \frac{I_{ph}}{eF} = \frac{\mu_h V}{L^2} (b\tau_e + \tau_h)$$

In this simplified picture, the gain increases linearly with the applied voltage bias and, assuming the electrodes can supply any required amount of current (ohmic contacts), it would seem that the gain could be made arbitrarily large. However, when the applied voltage becomes so large that the transit time is about equal to the dielectric relaxation time, τ_{REL}, which is a characteristic of the material, the current in the photoconductor will become space-charge limited and no further increase in the gain can occur. The maximum gain will then be obtained when the transit time is equal to the dielectric relaxation time and

is equal to the following.[6]

$$G_{MAX} = \frac{b\tau_e + \tau_h}{\tau_{REL}}$$

From the simple relations given, it can be seen that the performance of an ideal noiseless photoconductor is clearly described by its standard electrical properties and the excess carrier lifetimes.

3. Factors Which Affect Lifetime

In order to consider the factors which determine the excess carrier lifetime, it is first necessary to discuss the basic electronic transitions between different energy states. In a perfect semiconductor crystal structure of infinite dimensions, there are no allowed energy states between the top of the valence band and the bottom of the conduction band. Such a structure, of course does not exist and in general, a deviation of any kind from the perfect structure introduces discrete energy levels within the forbidden energy gap. These crystal imperfections include the surface of the material, vacant lattice sites, interstitial, substitional, or impurity atoms, and various dislocations and warping in the crystal structure. The energy levels created by these imperfections are localized within the crystal. When a charge carrier makes a transition to this energy level it is said to be captured and becomes a

---

[6] Rose, A., Concepts in Photoconductivity and Allied Problems, p. 7, Wiley, 1963.

bound charge at the site of the imperfection, no longer free to move about the lattice. For this reason, the discrete energy levels within the forbidden gap are considered to communicate only with the valence and conduction bands. Transitions between imperfection levels generally do not occur because of the separation in space of the locations of these levels.

The general energy band structure and the three major electron processes, excitation, capture, and recombination, are shown schematically in Fig. 2. Excitation occurs when an electron absorbs a photon and makes an upward transition in energy (1,2,3). Excitation may also occur due to thermal energy transfer if the two levels are close together in energy (4',5'). Capture occurs when a free electron makes a downward transition in energy either from the conduction band to an imperfection level (5,7) or from such a level to the valence band (4,6) which is actually the capture of a hole from the valence band. Recombination occurs when an electron makes a downward transition from either the conduction band or an imperfection level to the valence band where it joins with a hole or when an electron goes to an imperfection level already containing a captured hole (8,9,10). In these downward transitions, the excess energy is converted through the emission of a photon (luminescense) or of a phonon (lattice heating).[7]

---

[7] Bube, R. H., Photoconductivity in Solids, p. 38-46, Wiley, 1962.

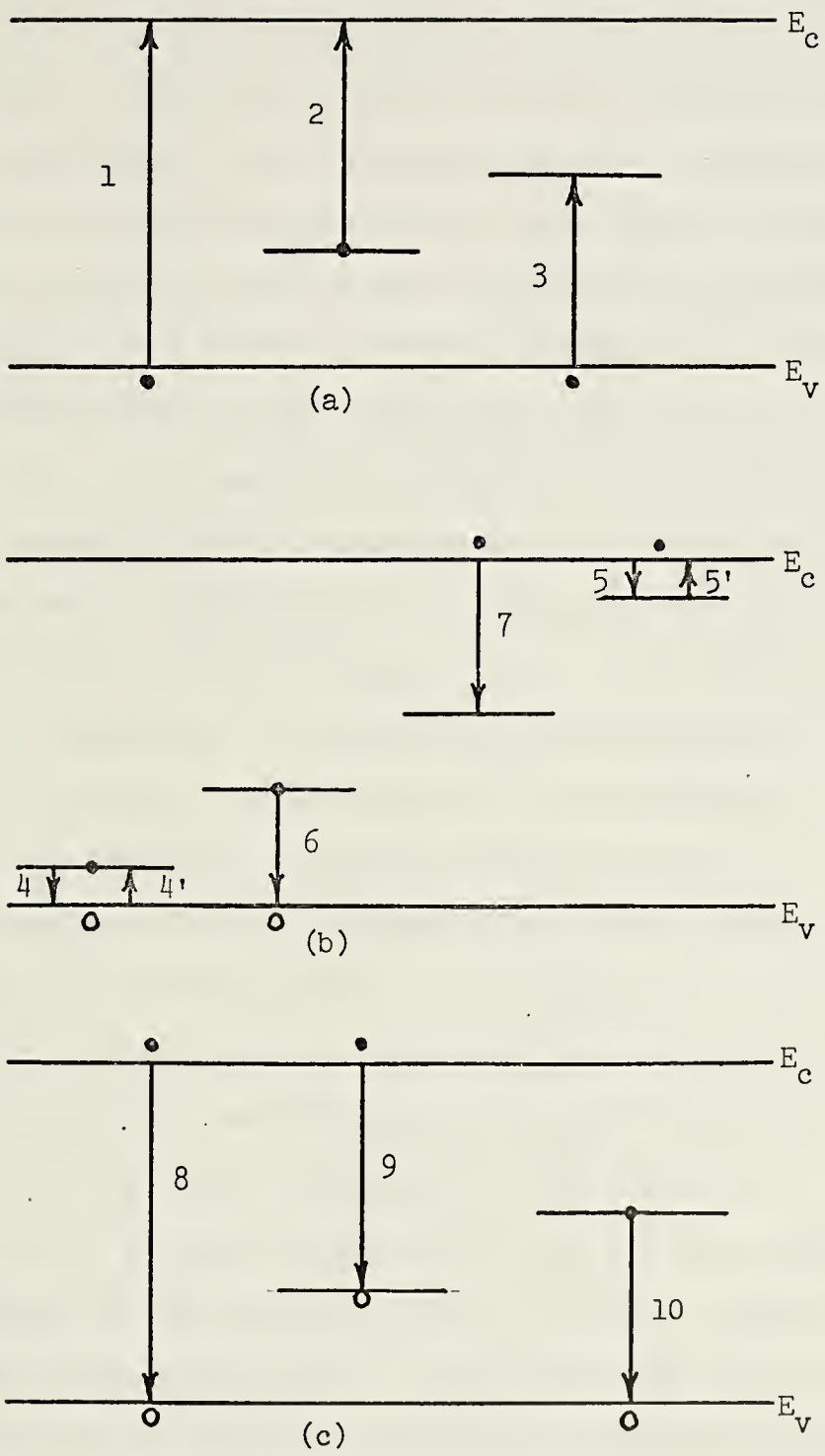

FIGURE 2. COMMON ELECTRONIC TRANSITIONS IN PHOTOCONDUCTORS: a) ABSORPTION AND EXCITATION, b) TRAPPING AND CAPTURE, c) RECOMBINATION (FROM REF. 15)

Based on these processes, capture centers can be classified into two general categories, traps and recombinations centers. Traps have energy levels which are close enough to a band edge that the probability of a captured carrier being excited back into the closer band by thermal energy is much greater than that of making the transition across the gap to the other band for recombination. Recombination centers have energy levels near the center of the forbidden band. If a carrier is captured in a recombination center, the probability of recombination occurring is much greater than the probability of the captured carrier being excited back to its original band. When a free carrier is trapped, its lifetime is only temporarily interrupted. It is only when recombination occurs that the lifetime of the free electron-hole pair is conclusively terminated.

The number of times a second that a free carrier comes close enough to an imperfection to be captured is the product of the capture center density (N_e and N_h), the capture cross sections (S_e and S_h), and the average thermal velocity of the carrier (v_e and v_h). The capture cross section is determined by the coulomb forces affecting a free carrier in the vicinity of the capture center. A single imperfection may act as a capture center for a free electron if its associated energy level is not occupied and as a capture center for a free hole if the level contains a captured electron. It is therefore necessary to distinguish between capture center densities and capture cross sections for electrons and those

for holes. If the capture centers are recombination centers, it can be assumed that the lifetime is terminated when capture occurs and the average lifetimes can be written as the following expressions.[8]

$$\tau_e = \frac{1}{N_e \, v_e \, S_e} \qquad \tau_h = \frac{1}{N_n \, v_h \, S_h}$$

For materials in which direct recombination between holes and electrons across the energy gap is an important factor such as is frequently the case in direct-gap semiconductors, a free hole can be considered as a form of mobile capture center with an associated capture cross section and density.

Therefore, it can be seen that the density of capture centers, their capture cross sections, and the statistics of their occupation are the most significant factors affecting the excess carrier lifetime. Changes in the occupation of the energy levels of various imperfections under different conditions of temperature and light intensity result in complex variations in lifetime, and consequently gain, over a wide range of values in a single photoconductor [Refs. 12 through 16].

4. Photoconductive Transient Response

As is the case in the analysis of any dynamic system, a great deal of information concerning the internal mechanisms

---

[8] Rose, A., Concepts in Photoconductivity and Allied Problems, p. 15, Wiley, 1963.

of the system can be obtained through observation of the transient response to a step input. The form of the transient response of a photoconductor is determined by the time rate of change of the excess carrier densities. In the most simplified mathematical model for this response, the rate of change of the excess electron density is assumed to be equal to the difference in the rate of generation of free hole-electron pairs (f) and the rate at which free electrons are removed from the conduction band. This very simple approach assumes that there is no trapping of free carriers. The rate of removal of electrons from the conduction band is written as the excess electron density divided by the average time each electron spends in the conduction band which is assumed to be a constant and equal to the lifetime. The resulting differential equation has a familiar basic form.

$$\frac{dn}{dt} = f - \frac{n}{\tau}$$

In the steady state, the rate of change is zero and the density of excess carriers has the dependence on lifetime and the generation rate as given before.

$$f - \frac{n_o}{\tau} = 0 \qquad n_o = f\tau$$

Solving the differential equation shows the response to a

step input to have a simple exponential dependence in which the time constant is equal to the lifetime.

$$n(t) = n_o(1 - e^{-t/\tau_o})$$

$$n(t) = n_o e^{-t/\tau_o} \qquad (f = 0)$$

$$\tau_o = \tau$$

In actual photoconductors, the factors which determine the transient response are much more numerous and have complicated dependencies on temperature, illumination intensity, and the excess carrier densities themselves. However, the time dependence of the rise and decay of the photoconductive response to a rectangular pulse input of radiation can usually be approximated by simple exponential functions. Since the time constants of these exponentials are determined by the rates of change of the excess carrier densities, they are indicative of the type of energy transition processes occurring in the material under the particular conditions.

One of the most interesting phenomena observed in photoconductors of lead salts and their alloys such as lead-tin selenide is that the decay time constant or relaxation time is generally much larger than the excess carrier lifetime indicated by the magnitude of the response. A simple explanation for this effect based on the trapping of minority carriers was first proposed by Bube [Ref. 15] and later

shown to apply to PbSe by Petritz and Humphrey [Ref. 17] and to other lead salts by Klaassen [Ref. 18]. This model assumes the energy band structure shown if Figure 3 in which electrons are specified as the minority carriers. There is a large density of traps which have a very high capture probability for electrons but are unattractive to holes even when containing a captured electron. The energy level of the traps, E_T, is assumed to be deep enough within the conduction band that the probability of a captured electron being excited to the conduction band by thermal energy is small. An electron will therefore remain in the traps a relatively long time once it has been trapped. Recombination is assumed to occur only directly between the conduction band and the valence band. However, the model may easily be applied to material in which there are a level of recombination centers. In this case, the density of majority carriers (holes) is assumed large compared to that of minority carriers so that the time an electron spends in a recombination center before recombining with a free hole is very short. Therefore, recombination can be considered to occur as soon as an electron is captured by a recombination level.

According to the model, electrons excited into the conduction band by incident photons are quickly trapped. The density of free electrons is small and the photoconductivity is mainly due to the excess free holes. There are very few electrons available to recombine with the excess holes, however, The rate of recombination becomes governed

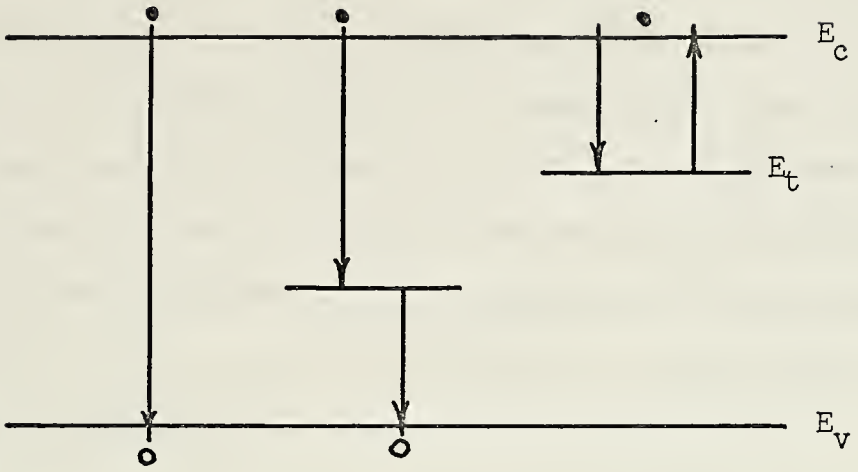

FIGURE 3. MINORITY CARRIER TRAPPING MODEL ENERGY BAND STRUCTURE

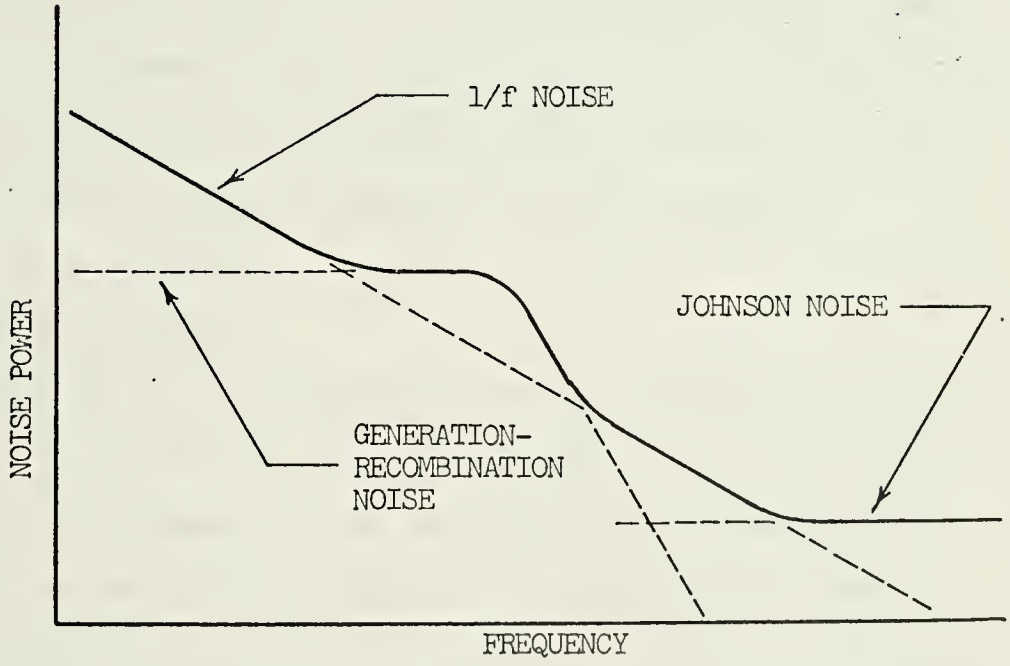

FIGURE 4. GENERALIZED DETECTOR NOISE SPECTRUM (FROM REF. 19)

by the rate at which electrons are released from the traps, which, as stated, is very slow. The result is that the decay time constant of the photoconductive response is about equal to the average time an electron spends in a trap (assuming re-trapping does not occur). This time may be much longer than the lifetime indicated by the magnitude of the steady state response of the material resulting in a decay time much greater than the lifetime.

B. NOISE IN PHOTOCONDUCTORS

The previous discussion was concerned with the sensitivity of photoconductors and entirely omitted any consideration of the noise which is an extremely important factor. The response of a photodetector can always be amplified by some active device, however, the noise in the detector limits the maximum signal to noise ratio which can be obtained at low radiation levels and makes detection of weak signals difficult or impossible.

1. Types of Noise

The noise in photodetectors has a variety of sources and forms. The four types of noise which are of major concern in the measurement of the response of infrared photoconductors, assuming all environmental electrical noise has been eliminated are briefly discussed in this section.

An unavoidable source of noise in all photodetectors is the background noise due to random fluctuations in the number of photons reaching the detector from all surrounding

objects which have a temperature greater than absolute zero. This noise imposes an upper limit, dependent on temperature and wavelength, on the detectivity of the detector. In practical photodetectors, however, other forms of noise predominate and the background noise serves only as a standard theoretical limit for comparison of performance.

Johnson noise or thermal noise is present in all conducting materials and is due to the random motions of electrons in the material. Johnson noise has a flat power frequency spectrum (white noise) and is independent of the current in the conductor. The r.m.s. value of the noise voltage (v_J is dependent on the absolute temperature (T), the resistance (R) and the noise equivalent bandwidth as shown in the well-known relation below in which k is the Boltzmann constant.

$$v_J = \sqrt{4kTR\Delta f}$$

Another type of noise has a power spectrum which varies as the inverse of the frequency and is referred to as 1/f noise. The primary source of 1/f noise is believed to be the breakdown of potential barriers which are formed within the bulk of the material and, much more significantly, at the contacts if they are not perfectly ohmic. Unlike Johnson noise, 1/f noise shows a strong dependence on the

current in the material and the noise power is generally found to vary as the square of the current.

The major source of noise in semiconductors at frequencies above those at which 1/f noise is significant is generation-recombination noise. This is due to random fluctuations in the rate of generation and of recombination of free hole-electron pairs and is similar to shot noise in vacuum tubes. It has a flat power spectrum out to a frequency equal to the inverse of the free carrier lifetime beyond which the power falls off rapidly.

A typical noise frequency spectrum which is a combination of these three major sources of internal noise is shown in Figure 4.[9] The actual frequency scale would vary with the type of detector and the temperature. Ideally, the detector would be operated at a frequency above those for which 1/f noise and generation-recombination noise are significant, but, of course, this is seldom possible.

2. Measurement of Noise

The noise in a photodetector is a critical part in its performance rating so the measurement of noise is an important factor in detector evaluation. Noise is a random process by definition and can only be dealt with in a meaningful way as power rather than as a deterministic voltage. In addition, the power may have a complicated dependence on

---

[9] Hudson, R.D., Infrared Systems Engineering, p. 30, Wiley, 1969.

frequency and other factors. For these reasons, consistent and accurate measurement of noise requires careful consideration.

Since all major forms of internal detector noise have a distributed power spectrum, measurement of a finite noise signal requires that the noise be passed through some kind of a bandpass network. The magnitude of the noise power transmitted by the bandpass filter (P_N) depends on the shape and magnitude of the noise spectrum (N(f)) and on the shape of the filter transfer function (T(f)) as shown below.

$$P_N = \int_0^\infty N(f)\, T(f)\, df$$

For the sake of simplicity, the noise spectrum is generally assumed to be flat within the bandpass range which can be approximated to arbitrary accuracy by selection of a narrow enough bandwidth. Making the further assumption that the gain of the bandpass filter is unity at the center frequency, the noise power at the output of the bandpass can be written as the product of the amplitude of the whitened noise spectrum at the center frequency of the bandpass filter (N_o) and the noise equivalent bandwidth (Δf).

$$P_N = N_o\, \Delta f$$

$$\Delta f = \int_0^\infty T(f)\, df$$

For a simple tuned circuit type of transfer function, the noise equivalent bandwidth can be shown to be $\pi/2$ times the half-power bandwidth given by the center frequency divided by the Q of the circuit.[10]

The noise is generally measured as a voltage at the output of the bandpass filter. However, since the voltage is also a random process, only the r.m.s. value of the noise has meaning. For the ideal flat noise power spectrum, the r.m.s. value of the noise voltage ($\bar{v}_N$) varies as the square root of the amplitude of the spectrum and the noise equivalent bandwidth. This voltage can be put into its most basic form by normalizing it to a one-Hz bandwidth by dividing by the square root of the noise equivalent bandwidth.

$$\bar{v}_N \sim \sqrt{N_o \, \Delta f}$$

$$\bar{v}_{NN} = \frac{\bar{v}_N}{\sqrt{\Delta f}}$$

Ideally, the noise voltage should be measured by a true r.m.s. meter. Frequently, however, the measurement is done with an average-reading meter which has a full-wave rectifier at its

---

[10] Davidson, J. J., "Average vs. RMS Meters for Measuring Noise," IRE Transactions on Audio, v. AU-9, p. 108-111, July, 1961.

input and which is calibrated to read the r.m.s. value of a sine wave. In this case, a correction has to be applied to the indicated noise since the meter is responding to an average value rather than the r.m.s. value. The correction is highly dependent upon the waveform of the noise voltage. Generally, this factor is derived based on the assumption the noise has a Gaussian distribution in amplitude [Ref. 20]. This derivation is carried out in Appendix A. The use of the concepts of noise equivalent bandwidth and the r.m.s.-correction factor makes it possible to make fairly reliable measurements of noise using standard laboratory equipment.

C. INFRARED DETECTOR FIGURES OF MERIT

A universal means of comparing the performance of infrared photo-detectors has been well established in the form of a standardized set of figures of merit. These are given a detailed description in Ref. 19 and Refs. 21 through 25 and in other publications on infrared technology and will be dealt with only briefly in this paper.

1. Standard Radiation Source

The starting point for a standardized means of evaluating the performance of infrared detectors is a standard source of infrared radiation. For this, the blackbody radiator is the obvious choice since its total radiant power and frequency distribution are known exactly and since the ideal blackbody radiator can be very closely approximated by laboratory blackbody sources. The total power, W (watts), incident on a detector of sensitive area A_D (cm^2) a distance

R (cm) from a blackbody radiator of area A_B (cm^2), emissivity ε_B, and temperature T_{BB} (°K) is given by the following well-known relationship based on the Stefan-Boltzmann equation in which σ is the Stefan-Boltzmann constant (5.67×10^{-12} $W\text{-}cm^{-2}\text{-}°K^{-4}$).

$$W = \varepsilon_B \cdot \frac{\sigma T_{BB}^4}{\pi} \cdot A_B \cdot \frac{A_D}{R^2}$$

In order to measure the response of the detector as an alternating voltage signal, the radiation is generally modulated using a mechanical chopper which is simply a slotted, circular blade driven at a constant speed by a motor and placed in front of the blackbody source aperture. When the blade is spinning, the detector is alternately exposed to the blackbody radiation from the source and from the chopper blade at temperature T_{CH} (°K). The previous expression can then be modified to give the peak-to-peak amplitude of the signal.

$$W_S = \varepsilon_B \cdot \frac{\sigma(T_{BB}^4 - T_{CH}^4)}{\pi} \cdot A_B \cdot \frac{A_D}{R^2}$$

Most devices used to measure the output signal of the detector measure only the amplitude of the fundamental frequency component of the response. For this reason, it is necessary to add a correction factor to the peak-to-peak amplitude. This factor is the ratio of the r.m.s. value of the fundamental component of the input waveform to the

peak-to-peak value. This factor (α_{CH}) depends on the waveform of the radiation signal produced by the chopper blade, and, therefore must be calculated for each particular source and chopper configuration (Appendix C). An additional correction factor is added to account for any absorption by optical windows between the blackbody and the detector (α_w). The final form of the radiation signal on the detector is the following expression.

$$W_S = \alpha_{CH} \cdot \alpha_w \cdot \varepsilon_B \cdot \frac{\sigma(T_{BB}^4 - T_{CH}^4)}{\pi} \cdot A_B \cdot \frac{A_D}{R^2}$$

2. Detectivity and Responsivity

Once the amplitude of the signal incident on the detector is known, the most basic figure of merit, the responsivity, R (volts/watt), can be calculated simply as the ratio of the detector signal, V_S (volts), to the input signal.

$$R = \frac{V_S}{W_S}$$

Responsivity, however, does not take into consideration the detector noise. The noise is accounted for in the noise equivalent power, NEP. This is the radiation power required to give a signal-to-noise ratio of unity and is written as the following expression.

$$NEP(Hz^{\frac{1}{2}} - w) = \frac{W_S}{V_S/V_{NN}}$$

In this expression, V_{NN} is the noise normalized to a one-Hz bandwidth. The NEP is an awkward figure of merit in that it is smaller for the better detectors. To avoid this, the NEP is simply inverted and called detectivity. Detectivity can be considered as the signal-to-noise ratio produced by an incident signal of one watt. Since the noise in a detector has been widely observed to vary approximately as the square root of the detector area, all detectors can be put on the same basis independent of their size by multiplying the detectivity by the square root of the detector area. This is the most important figure of merit and is referred to as D*.

$$D^* \ (\text{cm-Hz}^{-\frac{1}{2}}\text{-w}^{-1}) = \frac{V_S}{V_{NN}} \cdot \frac{\sqrt{A_D}}{W_S}$$

The noise generally varies as the bias current to a power greater than one and the signal varies approximately linearly with the bias current. This results in there being a particular current which gives the maximum signal-to-noise ratio and, consequently, which gives the best detectivity as shown in Fig. 5. The responsivity given for a detector is the value measured at the bias current which gives the best value of D*.

3. Spectral Response

Photoconductors are quantum detectors in that they respond to the number of incident photons rather than the intensity of radiation. In addition, photons with an energy

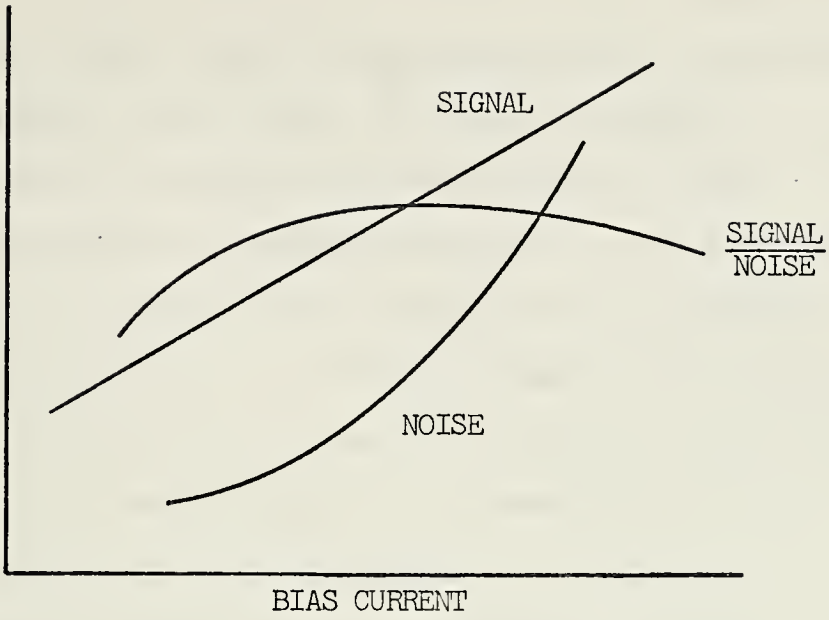

FIGURE 5. TYPICAL VARIATION OF SIGNAL-TO-NOISE RATIO WITH BIAS CURRENT

FIGURE 6. TYPICAL SPECTRAL RESPONSE FOR AN INTRINSIC PHOTOCONDUCTOR.

less than the band gap energy in intrinsic photoconductors (such as PbSnSe) cannot create free hole-electron pairs and will not be detected. For these reasons, the spectral response of quantum detectors is of interest in their performance evaluation. Spectral response is measured using a monochromator to separate the radiation from a wide-band source such as a glowbar, into a tunable band of wavelengths which can then be spatially filtered to irradiate the sample with a narrow band of wavelengths. The response of the detector versus the wavelength can then be recorded. Spectral response is indicated for a constant incident energy independent of the wavelength. Since the sources of radiation do not have such a flat radiation spectrum, the source must be calibrated using a thermal detector which has a flat spectral response. The response of the quantum detector is then normalized to a constant input power by dividing it by the thermal detector response at each corresponding wavelength interval. The resulting relative spectral response of a typical photoconductor is shown in Fig. 6. The rise in response with increasing wavelength is due to the fact that the number of incident photons must increase as the quantum energy decreases to maintain the same input power. Beyond the wavelength for which the photon energy is equal to the energy gap in the detector material, the response falls off sharply and the longer wavelengths cannot be detected.

IV. MEASUREMENT OF BLACKBODY RESPONSE, SPECTRAL RESPONSE AND PHOTOCONDUCTIVE TRANSIENT RESPONSE IN $Pb_{0.9}Sn_{0.1}Se$ THIN FILMS

A. BLACKBODY RESPONSE MEASUREMENTS

The photoconductive performance of the $Pb_{0.9}Sn_{0.1}Se$ thin films was determined through evaluation of the two basic photodetector figures of merit, responsivity and detectivity. These were determined through measurement of the response of the thin-film samples to radiation from a standard 500° K blackbody source. Since it is only necessary to measure two quantities, signal and noise directly from the sample itself, the evaluation of responsivity and detectivity is quite basic in theory. However, a meaningful evaluation of performance required establishing and maintaining the proper experimental conditions which increased the amount of equipment and effort involved. Since the response of the photodector was generally on the order of microvolts, extreme care and attention were required for accurate measurement and for elimination of numerous external sources of noise.

1. Measurement Apparatus

A block diagram of the blackbody response measurement system is shown in Fig. 7. Infrared radiation from a standard laboratory blackbody source was modulated using a mechanical chopper. The $Pb_{0.9}Sn_{0.1}Se$ sample was contained in a vacuum dewar, cooled by liquid nitrogen, and biased through an external supply. The signal was measured using

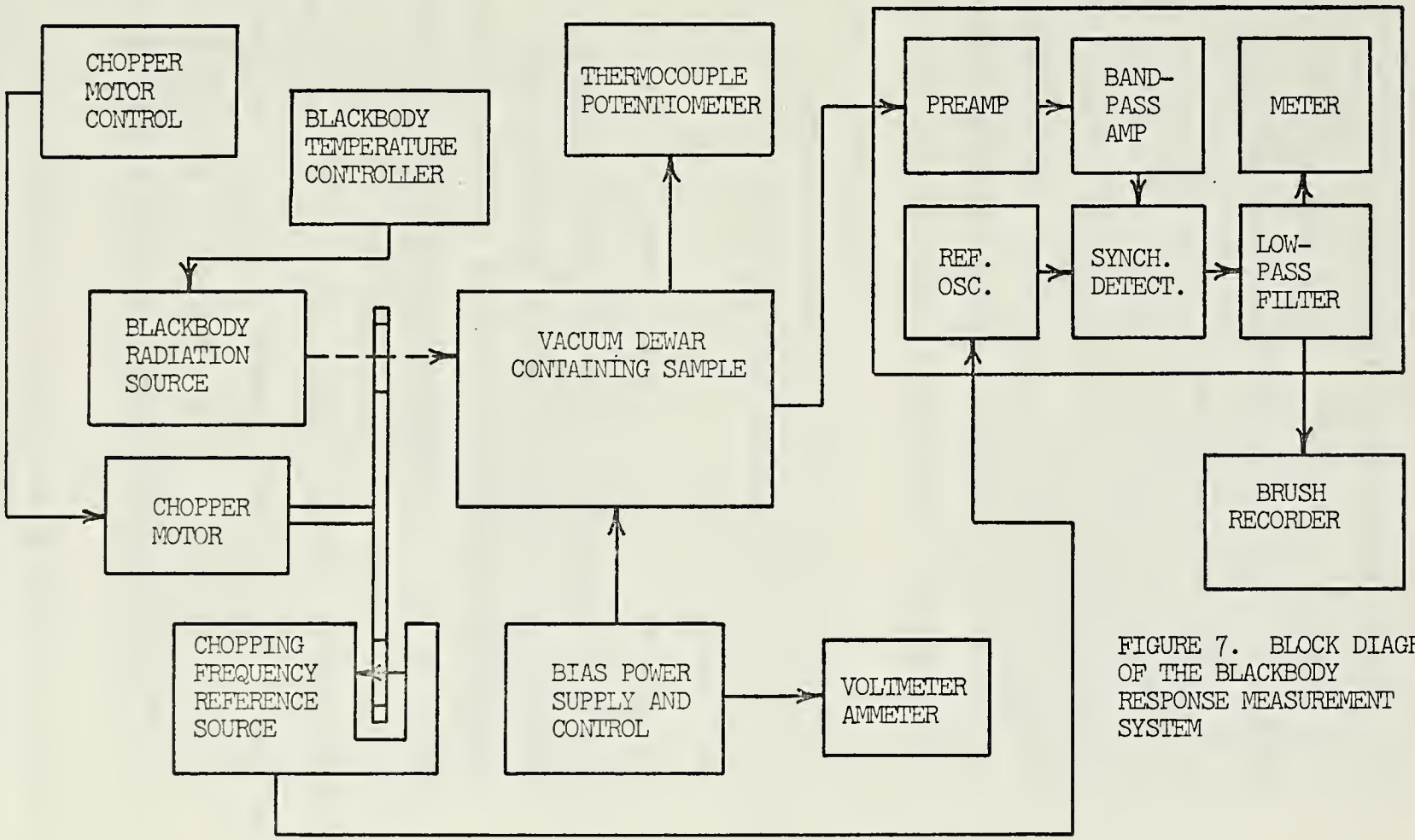

FIGURE 7. BLOCK DIAGRAM OF THE BLACKBODY RESPONSE MEASUREMENT SYSTEM

a lock-in amplifier (wave analyzer) with the synchronous frequency derived from an optical reference source at the chopper. The magnitude of the response signal was read from the amplifier meter or recorded using a strip-chart recorder. Photographs of the equipment are shown in Figures 8 and 9. The experimental apparatus used in the measurement of the blackbody response is divided into four main groups; 1) the vacuum dewar, 2) the bias circuitry, 3) blackbody radiation source and radiation modulation equipment, and 4) the signal measurement equipment.

a. Vacuum Dewar

Narrow-gap semiconductors such as lead-tin selenide are only effective as photoconductors at cryogenic temperatures. This is because at room temperature, the energy gap is only several times kT and the density of thermally-generated free carriers is so great that the presence of photo-generated excess free carriers is virtually undetectable. In this research, all photoconductivity measurements were made with the sample cooled by liquid nitrogen (boiling point 77° K) which required the use of a vacuum dewar. The vacuum chamber served the dual purpose of providing an insulation between the liquid nitrogen and the atmosphere and of preventing the formation of frost from water vapor in the air which would have ruined the sample.

Two different vacuum dewar designs were used in this research. A sectioned drawing of the dewar which was

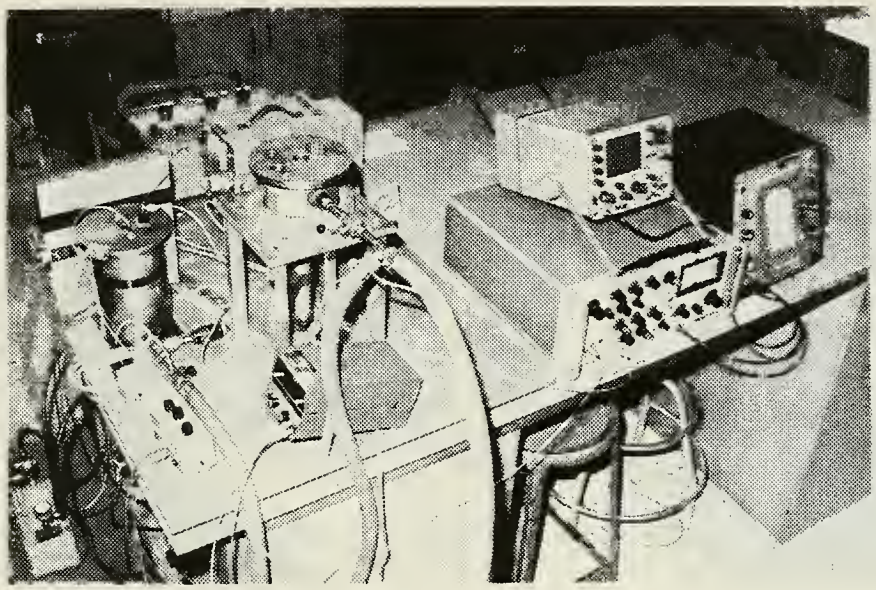

(a)

FIGURE 8. PHOTOGRAPHS OF THE EQUIPMENT USED IN BLACKBODY RESPONSE MEASUREMENT: (a) OVERALL SYSTEM, (b) LOCK-IN AMPLIFIER AND ASSOCIATED EQUIPMENT

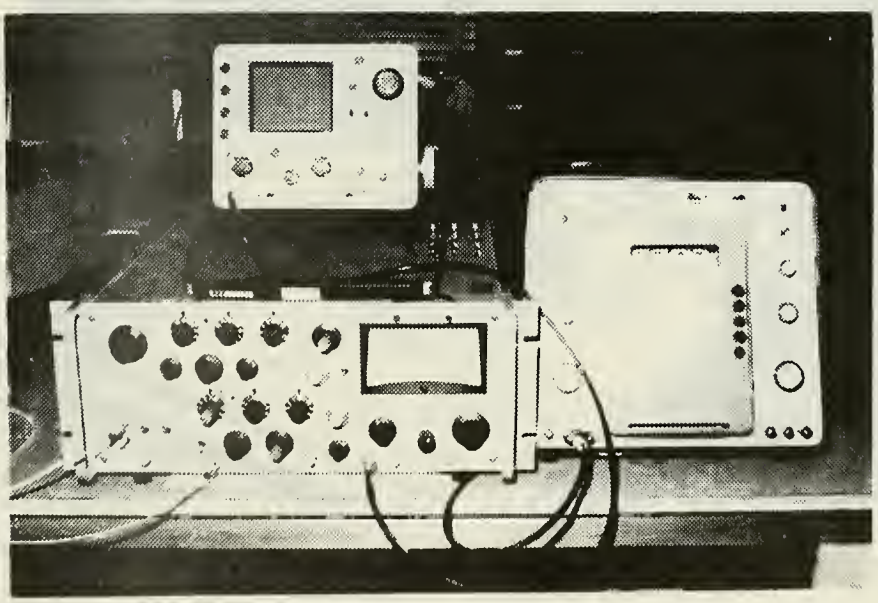

(b)

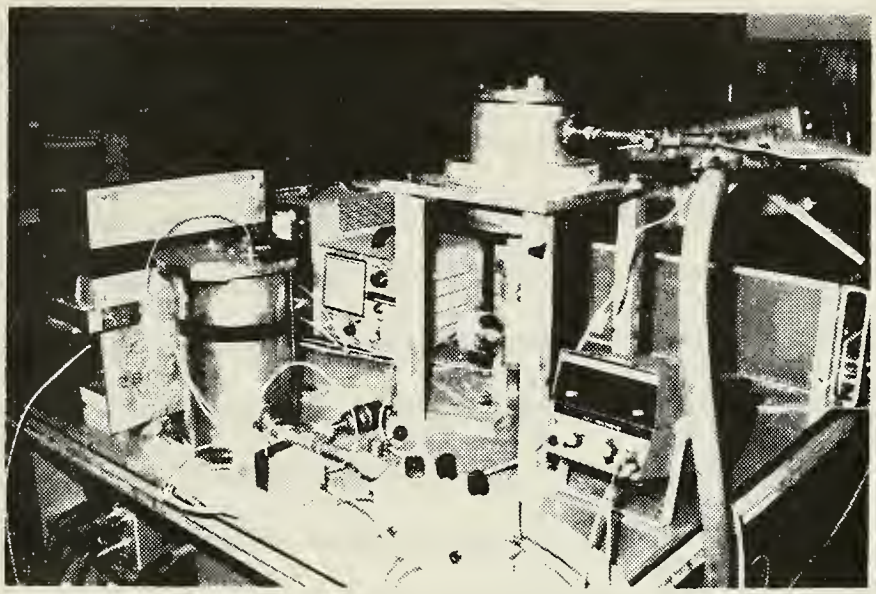

(a)

FIGURE 9. PHOTOGRAPHS OF EQUIPMENT USED IN BLACKBODY RESPONSE MEASUREMENT: (a) DEWAR AND BIAS CIRCUITRY, (b) BLACKBODY SOURCE, CHOPPER AND RELATED EQUIPMENT

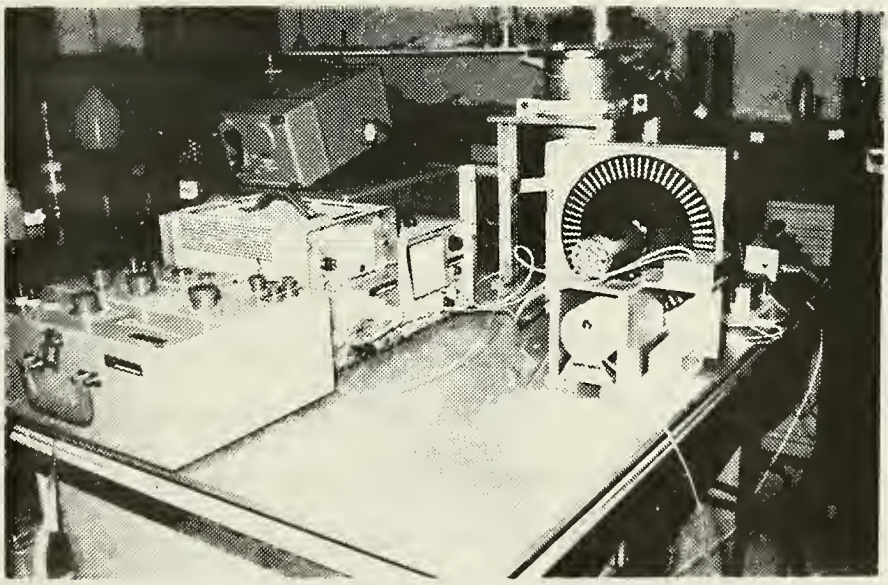

(b)

originally used is shown in Fig. 10. As shown, the sample was mounted using silicone thermal grease on one side of the copper cold-finger which was in contact with liquid nitrogen contained in the inner chamber. The cold-finger and liquid nitrogen reservoir were attached to the top cover plate and the whole assembly was removable to change the sample. A copper-constantan thermocouple was attached to a blank substrate on the other side of the cold-finger for monitoring the temperature of the sample. The sample was exposed to radiation through the KRS5 window which was made of thallium-bromide and had a flat spectral transmittance well beyond the cut-off wavelength of the samples.

This entire dewar and cold-finger arrangement was originally designed for electrical measurements based on the Hall effect which required the long tail section to place the sample between the poles of an electromagnet. Because of this, the original design was observed to have two major drawbacks. First, with the chopper motor in its original mounting arrangement, the blackbody source could only be placed 18 cm away from the sample which resulted in weak radiation intensity at the sample. Second, difficulties were encountered in maintaining temperatures below 110° K for the period of time required for carrying out a photo-response measurement. This was thought to be due to the insulating effects of ice which formed between the cold-finger and the liquid nitrogen when water which had condensed in the inner chamber froze.

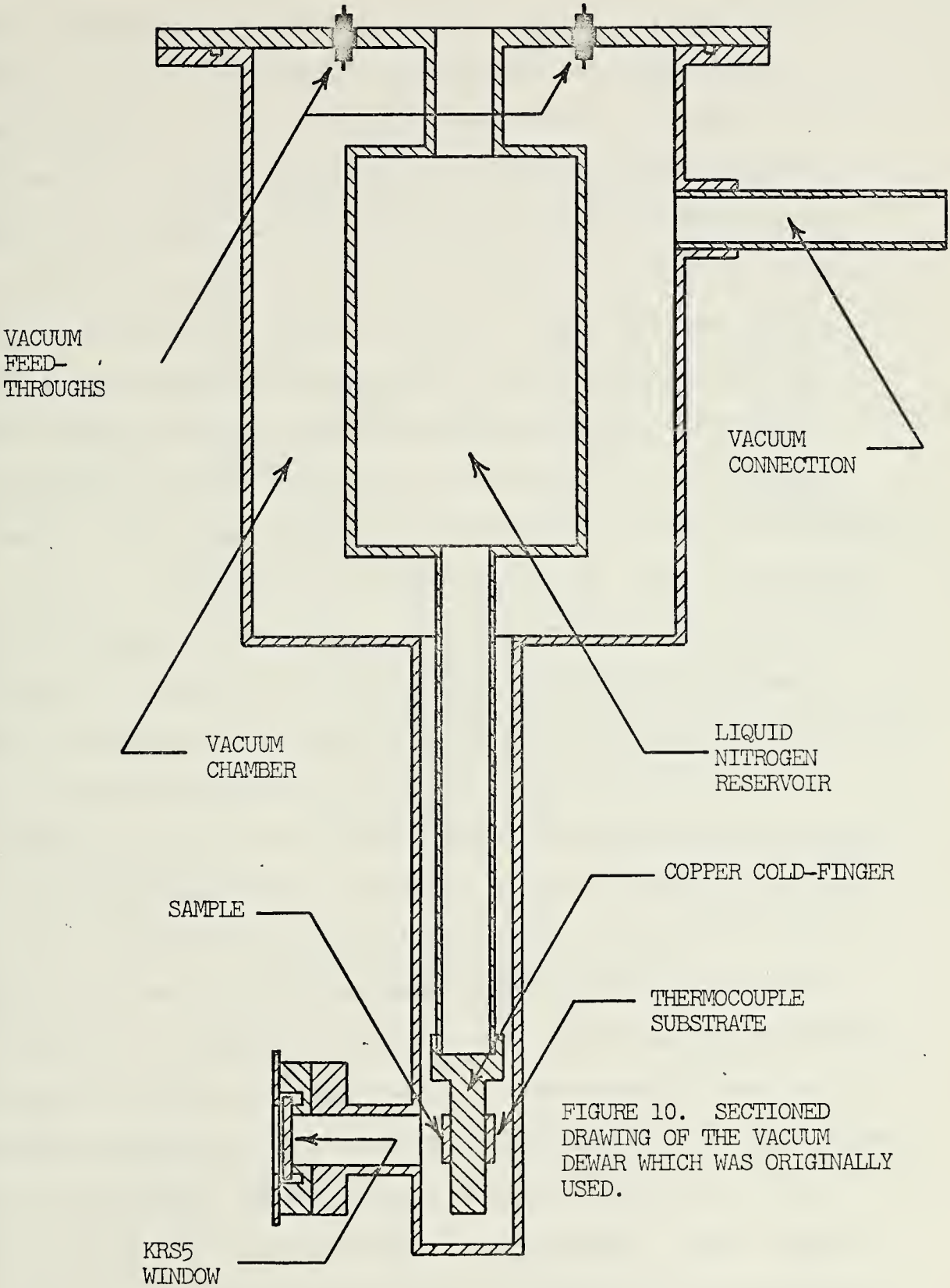

FIGURE 10. SECTIONED DRAWING OF THE VACUUM DEWAR WHICH WAS ORIGINALLY USED.

In an attempt to eliminate these problems, a new dewar shown in section in Fig. 11 was designed and built. In this new dewar, the sample and thermocouple were mounted on the face of a copper bar 1.5 inches in diameter. The bar extended well into the inner chamber and was in close contact with the liquid nitrogen through a number of holes drilled in the bar. The face of the bar was also close to the KRS5 window. Using the new dewar and a new mounting arrangement for the blackbody source and chopper shown in the photographs in Fig. 9, it was possible to place the source as close as 5.3 cm from the sample, resulting in over ten times more radiation intensity.

Although ice formation was no longer a problem, difficulties in achieving temperatures close to that of the liquid nitrogen were still encountered. In both dewars, when liquid nitrogen was first poured into the inner chamber, the temperature would go down to close to 90° K. The temperature would then rise slowly to around 115° K in spite of the fact that there was still plenty of liquid nitrogen in the reservoir. These difficulties were found to be partially due to a measurement problem. The thermocouple leads were brought to the outside of the dewar by connecting them to a vacuum feed-through. A thermocouple junction of polarity opposite to that of the junction on the cold-finger was unavoidably formed between the constantan wire and the inside lead of the vacuum feed-through. Since copper wires were originally used for both leads on the atmosphere

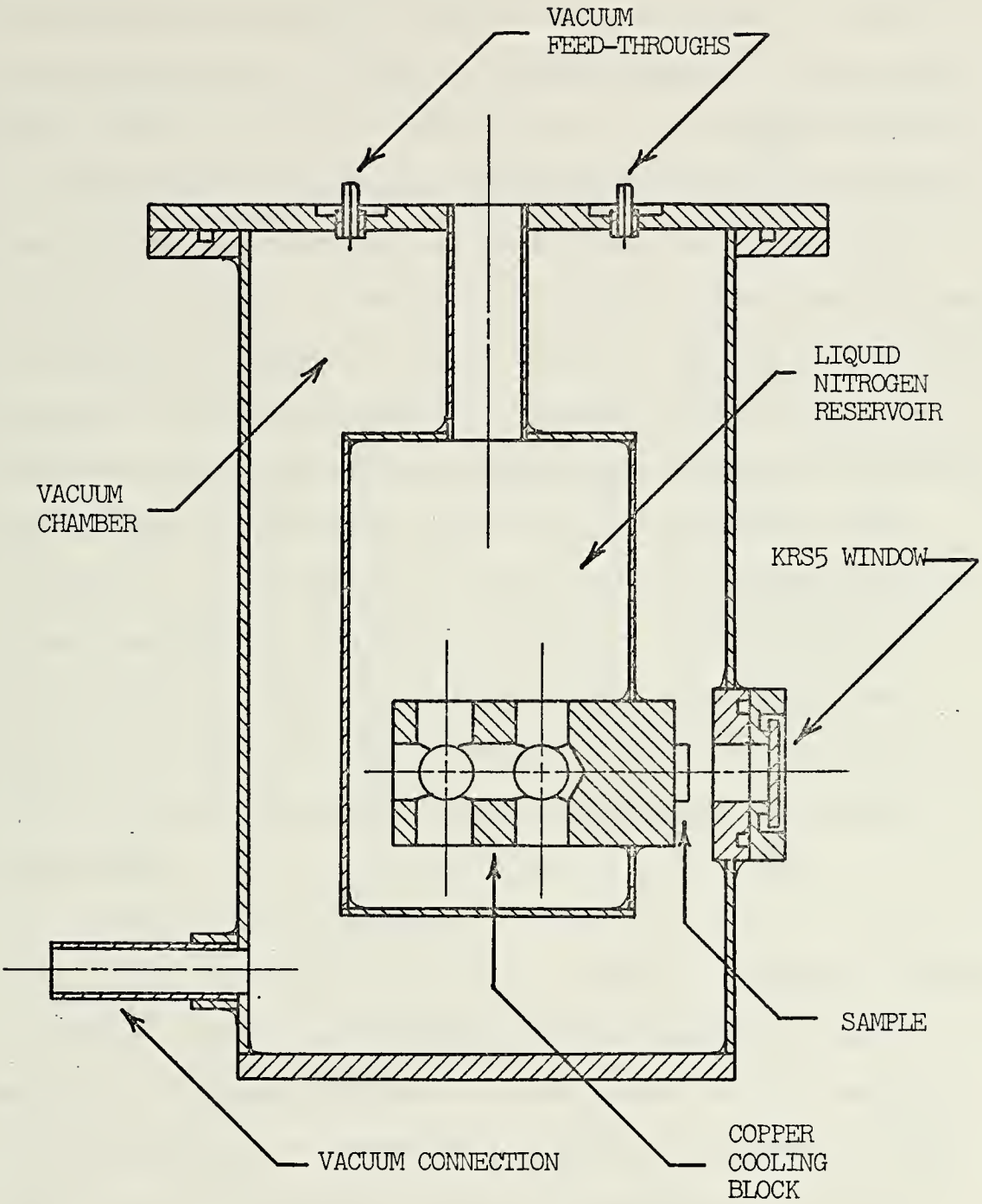

FIGURE 11. SECTIONED DRAWING OF THE NEW VACUUM DEWAR SYSTEM

side of the feed-through, the junction was not balanced by an equivalent junction at the same temperature. It was thought that when this junction was gradually cooled below room temperature by the thermal path to the liquid nitrogen, an increasing voltage was produced which caused the thermocouple potentiometer to read less than the cold-finger junction voltage. To help correct this, copper and constantan wires were used to connect from the outside of the feedthrough to the potentiometer. Insulation was used to help maintain both sides of the feedthrough, which were opposing thermocouple junctions, at the same temperature. This resulted in a considerably lower indicated temperature and it was possible to maintain the sample at temperatures around 95° K to 100° K for fairly long periods of time. The factors which prevented attaining temperatures down to 77° K, the boiling point of liquid nitrogen, were not determined.

b. Bias Circuitry

The bias circuitry was used to produce a constant, low-noise current in the sample. This circuit made it possible to detect changes in conductance of the sample as a voltage signal. A schematic diagram of the bias system as set up for blackbody response measurements is shown in Fig. 12. The system had three main components outside the dewar: the power source, the switch box, and the junction box. The power source was a standard laboratory power supply (0-500V, 0-100mA) with an external low-pass filter

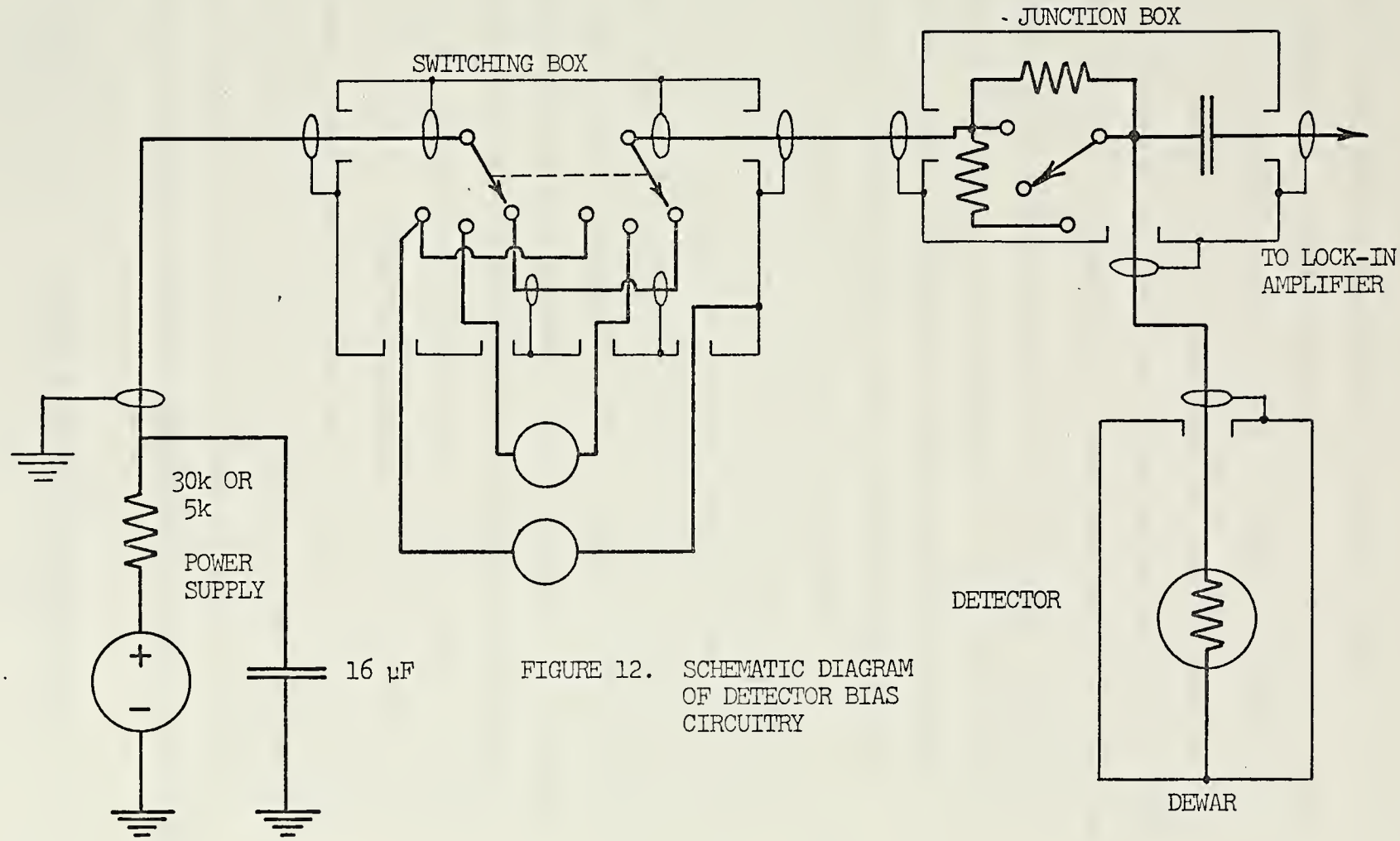

FIGURE 12. SCHEMATIC DIAGRAM OF DETECTOR BIAS CIRCUITRY

connected for additional filtering. Normally, batteries are used as a power source for photodetectors because, if fresh, they produce relatively less noise.[11] However, the large bias currents required for these samples made it difficult to maintain the batteries in fresh condition and the noise produced by the bias system using the power supply was observed to be approximately the same as that from the batteries. This was partially due to the fact that when using the power supply, the magnitude of the bias current could be varied by changing the supply voltage, thereby eliminating the requirement for a variable resistor in the circuit, generally a very noisy component.

The switch box following the power supply was included to make it possible to use a multimeter to measure the bias current through the sample or the voltage across it, or to completely eliminate the meter from the circuit when photoconductivity measurements were being made. The junction box contained the coupling capacitor for the signal output and a switch to select either a 3.8 k-ohm or a 15 k-ohm load resistor. When measurements were made using the first dewar, the load resistor was contained in the dewar at low temperature to reduce the thermal noise and external pickup. However, circuitry contained in the new dewar to be used for transient response measurements made it necessary

---

[11] Hudson, R. D., Infrared Systems Engineering, p. 335, Wiley, 1969

to put this load resistor outside of the dewar. The load resistor in the junction box could be shorted out with the switch when the d.c. voltage across the sample was measured to determine its resistance. The internal circuitry of the dewar consisted of two coaxial cables, one carrying bias current in and the blackbody response signal out, and the other carrying out the transient response signal from the 50-ohm impedance-matching resistor when these measurements were made.

c. Radiation Source and Modulation Equipment

The source of the infrared radiation used in this research was a standard laboratory blackbody radiation source (Barnes model 11-101T-1). This source had a fourteen degree conical cavity, a twenty degree field of view, and an emissivity of 0.99.[12] The blackbody source was maintained at a constant temperature by a Thermac controller and was set to within one degree of 500° K based on the measurement of the cavity surface using an iron-constantan thermocouple inserted through the aperature.

The radiation was modulated at one kHz by a chopper blade nine inches in diameter and with fifty slots. The blade was driven by an Electro-Craft motor-generator and speed controller. The chopper motor was mounted directly above the blackbody source on a metal stand which incorporated a heavy shield to protect the chopper blade.

---

[12] Wolfe, W. L., Handbook of Military Infrared Technology, p. 52, U. S. Government Printing Office, 1971.

The lock-in amplifier used to measure the signals from the irradiated sample required a reference frequency input of precisely the same frequency as the modulation. This was produced by an optical reference source mounted on the chopper stand so that the slotted chopper blade modulated the radiation from a light-emitting diode which illuminated a reverse biased silicon p-i-n diode. This circuit (Fig. 13) produced a signal sufficiently strong and free of harmonics to synchronize the lock-in amplifier reference oscillator.

d. Signal Measuring Equipment

The response of the thin film samples to the modulated blackbody radiation was generally a very small voltage on the order of microvolts accompanied by a large amount of wide-band noise. Accurate measurement of this signal required the use of a lock-in amplifier capable of detecting signals as low as a few nanovolts and sometimes buried deeply in noise. In this research, a Princeton Applied Research Model 124 Lock-In Amplifier with the Model 116 or the Model 118 Preamp was used for measurement of the signal and the noise [Ref. 27].

As shown in Fig. 7, the signal entered the lock-in amplifier at the preamplifier. This section provided an extremely low-noise amplification matched to a range of source impedances. The Model 116 Preamp was used in the transformer mode in which an impedance-matching transformer was placed between the source and the amplifier

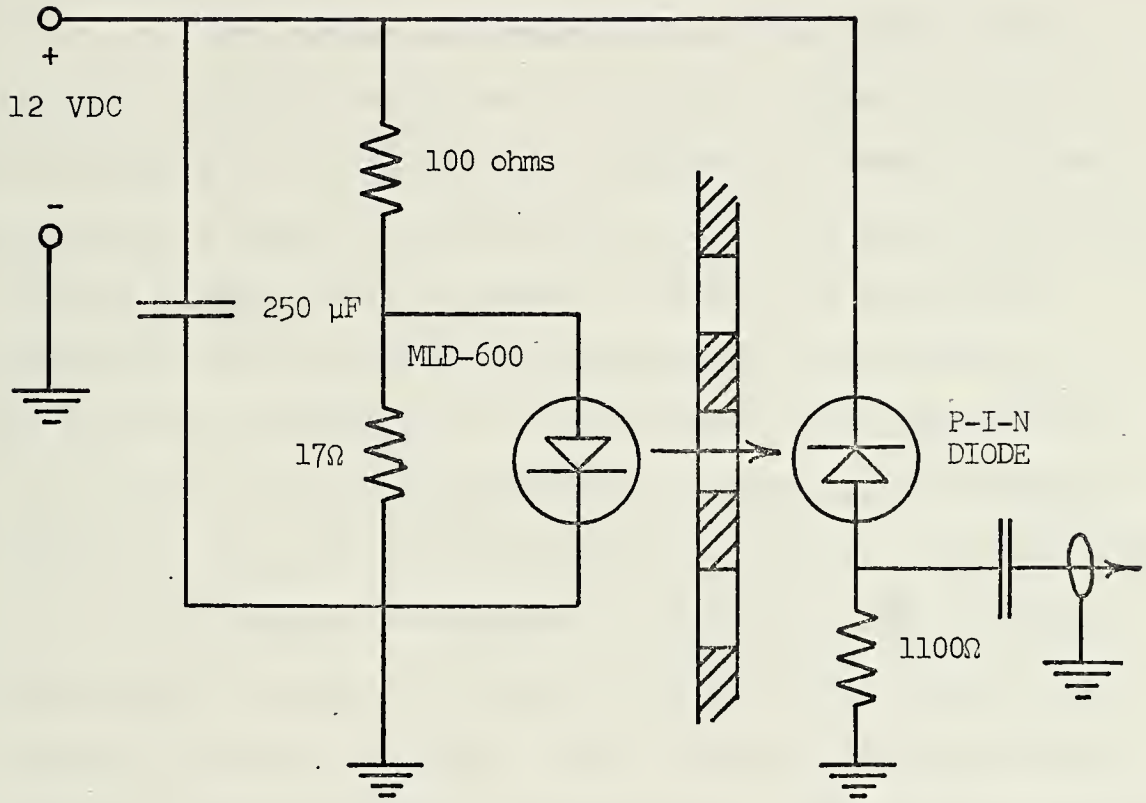

FIGURE 13. SCHEMATIC DIAGRAM OF CHOPPER FREQUENCY REFERENCE GENERATION CIRCUIT

for measurements on low-resistance samples. In this mode, the noise figure for the entire amplifier was less than 3 dB for source resistances from 6 to 600 ohms at a frequency of 1 kHz. The direct mode, in which the transformer was by-passed, was used for measurements of high-resistance samples and the noise figure was less than 3 dB for resistances greater than 1 k-ohm and less than 100 M-ohm.[13]

Following the preamplifier, the signal passed through a bandpass amplifier of variable center frequency and bandwidth to filter out all frequencies except the band in which the signal was expected to be. The signal was then fed into a synchronous detector in which the signal was multiplied by the output of an oscillator locked on to the reference frequency from the chopper. This converted the selected band of frequencies to an equivalent bandwidth centered at zero Hz by the heterodyne process. Any component of the input signal of frequency precisely equal to that of the reference signal was thereby converted to a proportional component of direct current. The output of the synchronous detector passed through a lowpass filter with a time constant which could be varied from 3 m-sec to 300 sec, so that all unwanted frequency components above zero Hz were eliminated. The output from the lowpass filter was indicated on an average-reading meter on the lock-in amplifier or recorded on a Brush strip-chart recorder. The lock-in amplifier

---

[13] Princeton Applied Research, Inc., Instruction Manual: Lock-In Amplifier, Model 124, p. III-10, 1971.

was calibrated using its own built-in voltage calibrator since a precision source of microvolt and nanovolt signals was not otherwise available.

The lock-in amplifier was also used to measure the detector noise. This was done with the amplifier operating in the ACVM mode in which the output of the bandpass amplifier passed directly to a full-wave rectifier and then to the lowpass filter and meter. The "10% ENBW" setting of the Q-selection dial was used to give an equivalent noise bandwidth of ten percent of the center frequency. This setting incorporated compensation for the difference between equivalent noise bandwidth and half-power bandwidth and for the error inherent in measuring a Gaussian process with an average-reading meter (Chapter II). Higher values of Q in the bandpass amplifier were frequently used for narrower bandwidths when it was desired to filter out specific frequency components such as the power line frequency and its harmonics. An oscilloscope was connected to the "SIGNAL" output of the lock-in amplifier to observe the signal before the synchronous detection or the noise before rectification.

2. System Noise Investigation

The noise in the measurement system was an extremely important factor in evaluation of photodetector performance. Since the response of the detector was generally only a few microvolts, excessive noise in the system would have made measurement of this signal very difficult and uncertain.

Also, since the noise from the detector itself was a significant factor in the figure of merit, detectivity (D*), it was important that the measured noise could be assumed to be mainly from the detector and that this noise could be measured without large error. For these reasons, the problems of noise measurement and external pickup were given careful consideration.

a. Johnson Noise Measurement and Noise Spectrum

The initial noise investigation was made using the lock-in amplifier to measure the noise in eight precision wire-wound resistors for which the noise output was assumed to be entirely Johnson or thermal noise. The resistors were connected at the input terminal of the amplifier and the noise was measured using four different center frequencies each with four values of Q in the bandpass amplifier section, and with the meter operating in the ACVM mode. This gave sixteen data points at ten different values of system bandwidth. The measured voltages were corrected for the amplifier noise figure which was approximately 1 dB over the range of resistances and frequencies used, and for the error due to the Gaussian nature of the noise as mentioned before. The theoretical Johnson noise and the measured noise were compared by plotting them versus the noise equivalent bandwidth on a log-log scale. This is shown in Fig. 14 for three values of resistance. As shown in the graph, the measured noise voltage varied directly with the square root of the noise equivalent

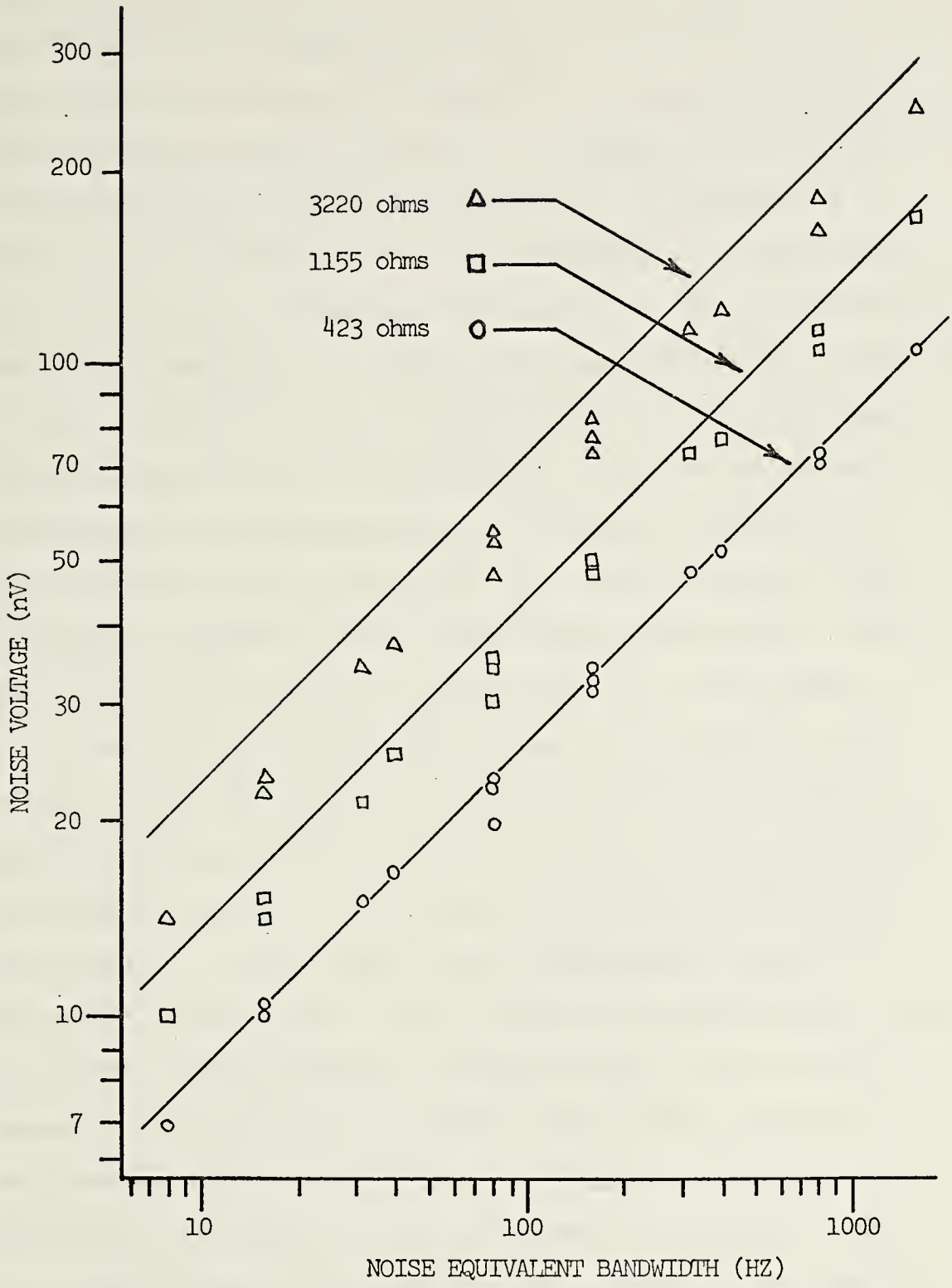

FIGURE 14. MEASURED AND THEORETICAL JOHNSON NOISE VERSUS NOISE EQUIVALENT BANDWIDTH FOR THREE RESISTANCES

bandwidth as predicted by theory. However, the measured and theoretical voltages differed by a ratio which was approximately constant for a given resistance, but varied from one resistance to another. The reason for the variation of this ratio with resistance was not determined. Errors due to calibration and/or difference in actual and indicated center frequency and Q of the bandpass amplifier would have resulted in a ratio that was more or less constant for all the resistances. It was thought that the typical noise figure curves for the lock-in amplifier which were supplied by the manufacturer were somewhat conservative when applied to the particular unit which was used, indicating more amplifier noise than there actually was. The noise figure was the only scaling factor in the system which had a dependence on the value of resistance. The ratios of measured noise to theoretical Johnson noise for the resistances used are listed in Table II along with the standard deviations of the data points about this ratio. The results of the Johnson noise measurements gave two important indications. First, since the maximum error was less than twenty percent, it appeared that noise could be measured by the lock-in amplifier with a fair amount of confidence, especially if order-of-magnitude accuracy was all that was needed.[14] Second, since the measured noise was always less than the theoretical noise, noise generation

---

[14] Brower Laboratories, Inc., A Practical Guide to Measurement of Weak Signals Buried in Noise, p. 22, 1968.

TABLE II

RATIO OF MEASURED NOISE TO THEORETICAL JOHNSON NOISE IN SEVEN RESISTORS

Resistance (ohms)	Ratio (V_M/V_J)	Standard Deviation (%)
423	0.97	4.6
830	0.91	5.4
1155	0.89	5.4
1650	0.87	4.8
2030	0.86	6.4
2590	0.85	5.5
3220	0.81	5.8

and pickup by the lock-in amplifier in this range of frequencies could be considered to be insignificant.

The success of any attempts to eliminate noise in the measurement system depended in part on the environmental noise present in the lab and not originating in the measurement equipment. To investigate this noise, measurements were made of the noise with a 20 ohm resistor in place of the sample in the dewar. Data was taken using a narrow bandwidth at various center frequencies from 5 Hz to 400 Hz. One set of measurements was made during the day with the overhead lights, the blackbody temperature controller, and two vacuum pumps operating. A second set was made late at night with all lights and other equipment turned off. The two noise frequency spectra obtained are shown in Fig. 15 in which the normalized noise voltage was plotted versus frequency. As expected, there were relatively strong noise components of power-line frequency and its harmonics present in both cases, although these components were considerably weaker in the quieted noise environment. It was found later that the strong harmonics of 60 Hz in the noisy environment originated mainly, if not entirely, in the blackbody source and its controller. The strong component of noise at the second and sixth harmonics of 60 Hz resulted from the extremely rapid rise of current in the power line when the triac in the controller turned on during both the positive and negative portions of each cycle. It was found that this noise could be almost entirely eliminated by

FIGURE 15. ENVIRONMENTAL NOISE SPECTRA IN NOISY AND QUIETED CONDITIONS

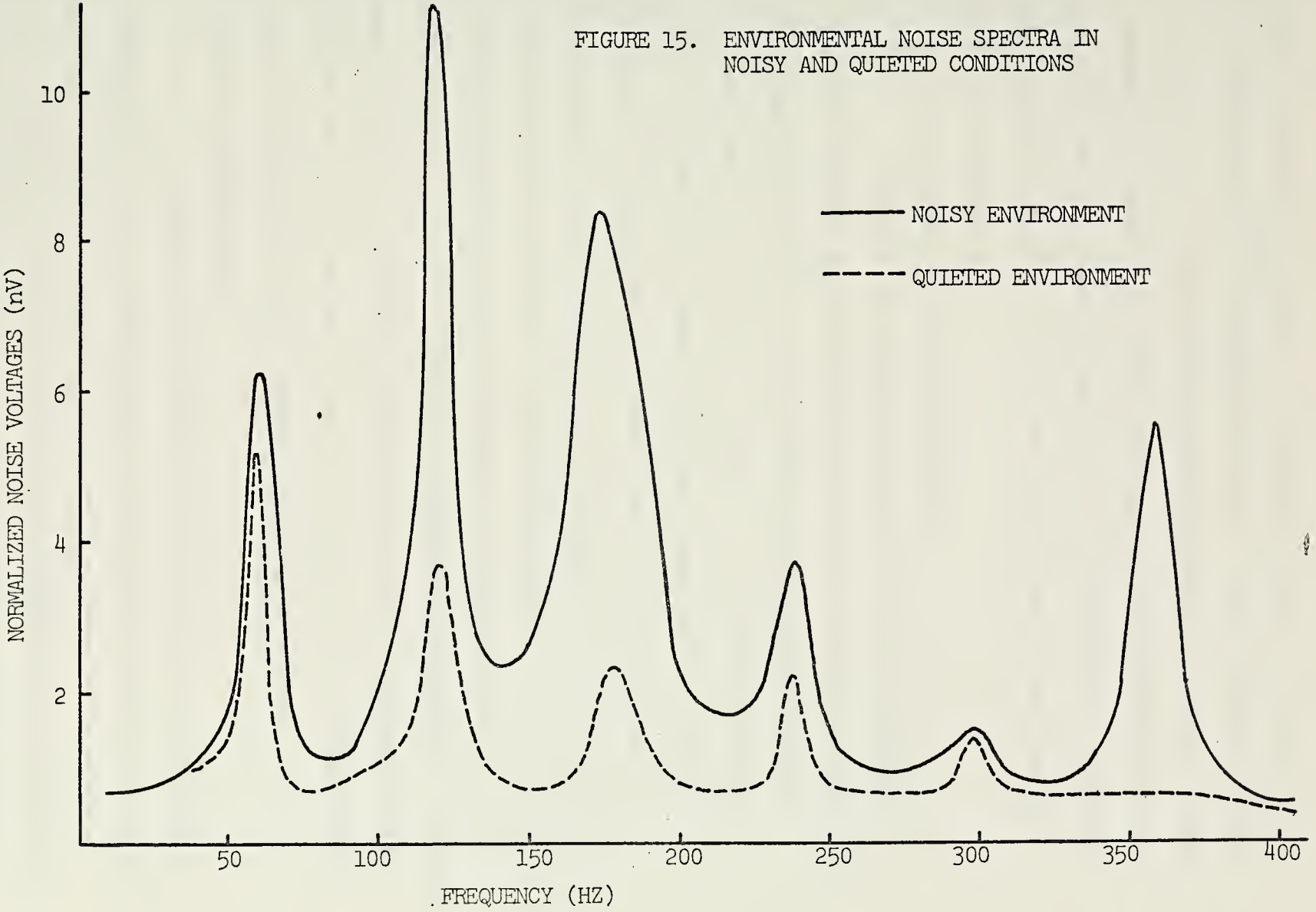

proper grounding as will be described later. Beyond 400 Hz, the power line frequency harmonics were not strong and it appeared that measurements could be made at these higher frequencies without concern with excessive external noise. Any measurements made below 400 Hz would have to be made with a narrow bandwidth and at frequencies other than 60 Hz and its harmonics.

b. Shielding and Grounding

Proper shielding was an extremely important consideration in reducing external noise pickup. According to universal practice, all signal-carrying leads were shielded coaxial cable. The type used was Microdot low-noise, 50-ohm cable made with high resistivity Teflon dielectric which allowed a very small shield diameter (0.1 inch). This cable also had powdered graphite between the dielectric and shield to reduce static electricity caused by cable flexing, a potential source of noise. All leads in the bias circuit from the power supply to the sample were also Microdot cable with the exception of those inside the junction box (Fig. 12) which was an electrically-sealed enclosure using coaxial feed-throughs at all external connections.

The lock-in amplifier was capable of excluding practically all random noise of continuous frequency distribution but was naturally extremely sensitive to any noise with a finite frequency component at the chopping frequency. For this reason, special efforts were required to reduce

leakage from the frequency reference circuit into the signal channel. As originally mounted on the chopper stand, this circuit had no shielding and used an open two-wire connection to its power supply. This configuration was very effective in transmitting a signal synchronous with the chopping frequency into the signal channel. Careful shielding of the reference frequency circuit, use of a shielded cable to its power supply, and incorporation of a lowpass filter between the circuit and power supply reduced the synchronous noise entirely.

The grounding arrangement for the equipment in the measurement system was probably the most important factor in making the system as free of noise as possible. When the entire measurement system was originally assembled, a resistor was mounted in the dewar in place of the sample to determine the system noise. The system was found to be completely inundated with power line harmonic noise. The reason for this turned out to be much simpler than the effort required to determine it and correct it would seem to indicate. A portion of the noise was eliminated simply by shifting the blackbody controller's power cord from the bench supply to a nearby wall outlet, although the reason for the improvement was not known at the time. Another large part of the noise disappeared when the metal legs of the blackbody source were insulated from the metal base-plate on which the dewar and chopper stand were mounted. Apparently, a strong electromagnetic field was generated

by rapidly switching current in the heating coils of the blackbody source. It was thought that this field gave rise to electric currents through the loop of the metal legs and base-plate which propagated into the signal channel through the dewar. Replacing the metal legs with ones made of plexiglass solved the problem and turning on the blackbody and controller no longer caused substantial increase of the noise level.

The other equipment, however, still introduced an unacceptably high amount of noise into the signal channel. The contribution of each piece of equipment was determined by the change in the noise which resulted when each was turned off. These noise voltages, measured with a Q of 20 and a center frequency of 1 kHz, are listed in the first column of Table III. (Noise is usually normalized to a 1-Hz noise equivalent bandwidth. However, this is only meaningful for noise with a flat frequency spectrum which was decidedly not the case here. Also, for Gaussian noise, the voltages are generally added as the square root of the sum of the squares, since noise power is the only truly meaningful quantity. The noise being measured was most likely not Gaussian in this case, and, for the sake of simplicity, the voltages measured were considered to add directly.) It was at this point in the investigation that it was learned that the bench power outlet was on an ungrounded power distribution system while the wall outlet was, of course well grounded. Placing all of the measurement

TABLE III

NOISE CONTRIBUTIONS OF EQUIPMENT IN THE MEASUREMENT SYSTEM FOR TWO DIFFERENT GROUNDING SYSTEMS

334 ohm resistor in the dewar, f_o = 1 kHz, Q = 20

Noise Source	Noise with un-grounded pwr. syst. (nV)	Noise with grounded pwr. syst.
Bias Power Supply	300	0
Chopper Motor and Controller	390	20
Reference Freq. Source Pwr. Sup.	200	6
Vacuum Pump	0	0
X-Y Chart Recorder	15	0
Brush Strip-Chart Recorder	65	4
Oscilloscope	10	0
Digital Multimeter	25	0
Digital Thermocouple Meter	55	0
PAR Lock-In Amp	44	0
Theoretical Johnson Noise	21	21
Total Measured Noise	1150	51

equipment on the grounded system resulted in a decrease in the noise level of more than an order of magnitude. The contributions of each piece of equipment with this improved grounding arrangement are listed in the second column of Table III.

In the measurement of voltages in the millivolt or microvolt range, the problem of ground loops can generally be neglected. However, in measurement of voltages on the order of fractions of a microvolt, the problem requires special consideration. A ground loop is defined as any conducting closed path in the grounding network through which currents generated by stray electromagnetic fields can flow such as the loop shown in Fig. 16-a. In this case, currents flowing in the loop produce a voltage drop E_{gl} between the two ends of the shield on the signal cable which causes the measured voltage to be E_s plus E_{gl}.[15] The preamplifier of the lock-in amplifier was designed to help eliminate the effects of the ground loop by using a differential input amplifier. As shown in Fig. 16-b, a 10 ohm resistor was connected between the inverting input and the ground. The result was that most of the potential drop in the ground loop appeared across the resistor where its effect was eliminated by the 120-dB common mode rejection

---

[15] Brower Laboratories, Inc. A Practical Guide to Measurement of Weak Signals Buried in Noise, p. 14-15, 1968.

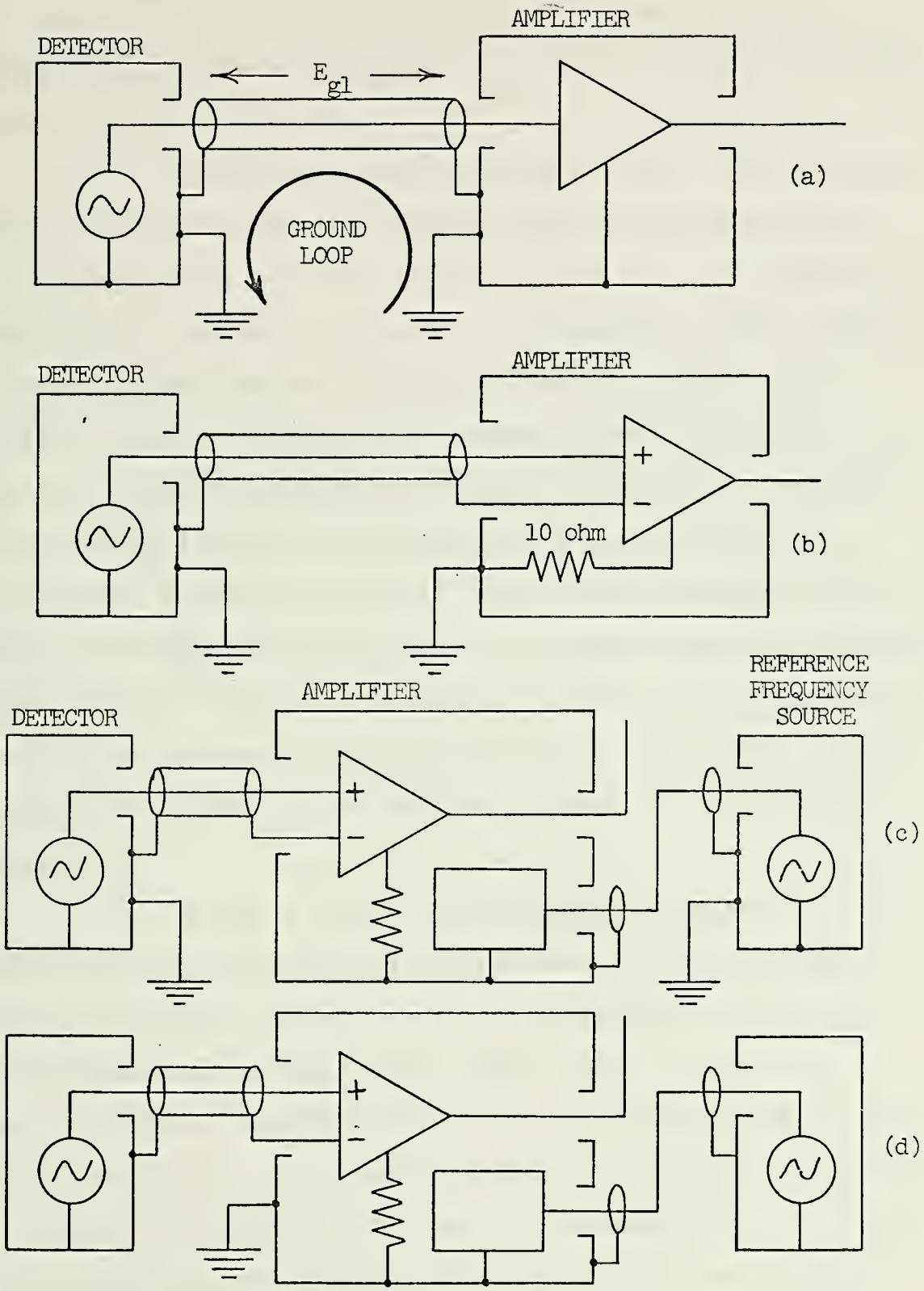

FIGURE 16. SCHEMATIC REPRESENTATION OF VARIOUS GROUND LOOPS

of the differential input amplifier.[16] Even with this provision, it was recommended that ground loops be avoided if possible.

The measurement system using the first dewar and chopper stand had an unavoidable ground loop as shown in Fig. 16-c, since both the chopper stand and the dewar were grounded to the metal base-plate on which they were mounted. However, since the measured noise was only a few times greater than the theoretical Johnson noise of the resistor in the dewar, the differential amplifier scheme was apparently effective and this particular ground loop was not considered a serious problem. When the measurement system was set up using the new dewar and chopper stand, the ground loop was eliminated by insulating the dewar and all associated bias circuitry from the base-plate (Fig. 16-d). This arrangement proved to be somewhat better in eliminating noise.

Based on their low-temperature resistance, the samples fell into two main categories; the low-resistance samples were all around one to three hundred ohms and the high-resistance samples were in the range from ten to twenty k-ohms. External noise pickup of the system in its final configuration was evaluated using a resistor in each of these ranges mounted in place of the sample in the dewar. The normalized noise measured with a 370 ohm resistor was

---

[16] Princeton Applied Research, Instruction Manual: Lock-In Amplifier, Model 124, p. III-4, 1971.

2.8 $nV/Hz^{1/2}$, approximately equal to the theoretical Johnson noise, 2.2 $nV/Hz^{1/2}$. With a ten k-ohm resistor in the dewar, the noise measured was 26 $nV/Hz^{1/2}$, two and a half times Johnson noise, 10 $nV/Hz^{1/2}$. This noise fell to 12 $nV/Hz^{1/2}$ when the blackbody controller was turned off, indicating that this was the major source of the excess noise. The noise contributed by the power supply was measured by observing the increase in noise when current was flowing in the resistors. There was no noticable increase in noise using the 370 ohm resistor. However, with the ten k-ohm resistor an increase in noise of approximately 15 $nV/Hz^{1/2}$ per milliampere of current was found. Since the high-resistance samples typically had high noise outputs on the order of several microvolts and were biased with only a few milliamperes of current, the larger amount of noise measured with the ten k-ohm resistor was considered as relatively insignificant.

3. Blackbody Response Measurement Procedure

The procedure for evaluation of detectivity and responsivity for the $Pb_{0.9}Sn_{0.1}Se$ samples had three phases: preparation, measurement, and calculations.

a. Preparation

The preparation for the measurement started with mounting the sample on the copper cold-finger in the original dewar or face of the copper block in the second dewar, using silicone thermal grease as an adhesive and thermal connection. The two wires used to pass current

through the sample in the Hall-effect measurements (contacts 1 and 5 in Fig. 1) were connected to two terminals on the mounting surface using low-temperature indium-alloy solder and the remaining six leads were clipped off. The two parts of the dewar were then put together and the vacuum chamber was evacuated to twenty microns Hg or less. The blackbody controller was adjusted so that the blackbody source had a temperature within one degree of 500° K and enough time was allowed for the source to stabilize at this temperature. Once a sufficient vacuum had been attained, liquid nitrogen was poured into the reservoir and the sample was cooled to as low a steady-state temperature as possible.

The chopper motor was turned on and given sufficient time to warm up. It was then adjusted to produce a chopping frequency as close as possible to 1 kHz by comparing the output of the chopped reference source to a 1 kHz signal from the lock-in amplifier's internal oscillator on an oscilloscope. It was necessary to repeat this adjustment periodically throughout the measurement since the chopper motor had a tendency to wander from its set speed. Although the lock-in amplifier would easily synchronize with a reference signal over a wide range of frequencies, the center frequency of the bandpass amplifier was fixed at 1 kHz. To reduce any phase shift and attenuation of the detector signal in this section of the amplifier, the chopping frequency had to be maintained close to 1 kHz.

b. Measurement

Only two quantities had to be measured from the sample, the response signal amplitude when the sample was exposed to the modulated blackbody radiation and the noise voltage from the sample when the radiation was blocked. These two quantities were measured for various values of bias current in an effort to find the best signal-to-noise ratio. Once the steady-state low temperature had been reached, the resistance of the sample at this temperature was determined by passing one milliampere through the sample and measuring the voltage across it. Based on this resistance, a starting bias current was selected which was generally five milliamperes for the low-resistance samples and one milliampere for the high-resistance samples. The current was controlled by adjusting the power supply voltage while watching a milliammeter switched into the circuit at the switching box (Fig. 12). When detector measurements were taken, the meter was switched out of the circuit so that all leads were shielded to prevent noise pickup. If this was not done, the open wires running to and from the milliammeter alone introduced so much noise into the system that the lock-in amplifier was overloaded on the five millivolt scale.

The detector signal was recorded as the average indicated value on the amplifier meter with the sample exposed to the modulated radiation and with the amplifier in the phase-sensitive detection mode. The lowest possible Q

was used on the bandpass amplifier to alleviate the attenuation and phase-shift problem described before. However, values of Q lower than ten generally let so much noise pass that the amplifier was overloaded. The phase control for the reference oscillator was adjusted for a peak meter indication at the start of each measurement. For all but the least sensitive samples, the meter indication was very steady when a time constant of one or three seconds was used on the low-pass filter. Once the signal voltage was recorded, the radiation was blocked to ensure that the amplifier indicated zero signal and that there was no synchronous noise present causing a zero offset error. When samples of very low sensitivity were measured using the first dewar and chopper stand arrangement, the meter reading varied considerably and there was an indication of some synchronous noise in the signal channel. To overcome these problems, the strip-chart recorder was used to record the output of the amplifier over a period of one minute or longer with the sample illuminated and with the radiation blocked. The two traces were then averaged graphically and the signal amplitude was taken as the difference between the two traces. Using the new dewar and chopper stand arrangement, however, signal voltages as low as 40 nV were measured with a very steady meter indication and no zero-signal offset error. The use of the chart recorder was never required. One sample which was considered to be insensitive as a result

of measurements made with the first system was shown to have a weak but definite sensitivity when re-evaluated with the new arrangement.

The lock-in amplifier was then switched to the voltmeter mode with the bandpass amplifier Q set to the ten percent noise equivalent bandwidth value. The noise was recorded directly as normalized noise. (With a center frequency of 1 kHz, the noise bandwidth was 100 Hz so the meter reading was simply divided by 10 $Hz^{1/2}$.) During the progress of the measurements, the sample temperature and blackbody temperature were monitored to ensure that they did not deviate significantly from the recorded values. Once the optimum bias current for a signal-to-noise ratio was found and the corresponding signal and noise voltages were recorded, the measurement was essentially completed.

c. Calculations

The calculations of responsivity and detectivity were done by entering the values of signal and noise voltages and of the experimental parameters recorded in the measurement phase into the standard relationships given in Chapter II. Before this could be done, however, it was necessary to apply two corrections to the measured values of signal and noise. The first correction was to account for the attenuation of the signal caused by the load resistor. Since the change in conductivity of the sample was detected as a change in the voltage across it, ideally the bias current should have been perfectly constant which would have

required an infinite load resistance. Using a constant supply voltage and a finite load resistance resulted in a lower signal than would have been observed under the ideal conditions. The simple correction used which is shown below is derived in Appendix B. Since the detector noise dominated the measured noise, this was considered as a form of signal from the detector which suffered the same attenuation and required the same correction. The second correction factor was applied only to the measured noise. It was done to take the lock-in amplifier noise into account using the noise figure contours supplied with the amplifier. The following is a summary of the relations and constant values used in the calculations.

$$V_S = V_{SM} \cdot (1 + \frac{R_D}{R_L})$$

$$V_N = V_{NM}(1 + \frac{R_D}{R_L}) \; / \; (\log_{10}^{-1} (NF/20))$$

V_{SM} = measured signal voltage.

V_S = corrected signal voltage.

V_{NM} = measured normalized noise voltage.

V_N = corrected noise voltage.

R_D = detector resistance at measurement temperature.

R_L = load resistance.

N_F = lock-in amplifier noise figure.

$$P_S = \alpha_{CH} \cdot \alpha_W \cdot \varepsilon_B \cdot \frac{\sigma(T_{BB}^4 - T_{CH}^4)}{\pi} \cdot A_B \cdot \frac{A_D}{d^2}$$

$$R = \frac{V_S}{P_S} \qquad D^* = \frac{V_S/V_N}{P_S} \cdot \sqrt{AD}$$

P_S = r.m.s. value of fundamental component of modulated radiation signal (watts)

R = responsivity (volts/watt)

D^* = detectivity ($cm\text{-}Hz^{-1/2}\text{-}W^{-1}$)

α_{CH} = form factor for the chopper waveform (0.375)

α_W = transmittance of the KRS5 window (0.7)

ε_B = emissivity of the blackbody source (0.99)

σ = Stefan-Boltzmann constant (5.67×10^{-12} $W\text{-}cm^{-1}\text{-}°K^{-4}$)

T_{BB} = blackbody temperature (° K)

T_{CH} = chopper blade temperature (° K)

A_B = blackbody aperature area (0.4 cm^2)

A_D = detector sensitive area (0.2 cm^2)

d = distance from balckbody source aperature to the detector (18 cm for the first dewar and chopper stand and 5.3 cm for the new arrangement)

The chopper form factor α_{CH} was the ratio of the r.m.s. value of the fundamental component of the signal waveform produced by the chopper to the peak-to-peak amplitude of this signal as described in Chapter II. It was derived as indicated in Appendix C based on the dimensions of the slots in the chopper blade and of the blackbody source aperature. The transmittance of the window was specified

by the manufacturer and was verified as a conservative value in terms of detector performance by measurement on a Perkin-Elmer spectrophotometer. The temperature of the chopper blade was taken as room temperature since this was the lowest probable temperature of the blade and the difference between the blackbody and chopper temperatures was no greater than that based on this assumption.

B. MEASUREMENT OF SPECTRAL RESPONSE IN $Pb_{0.9}Sn_{0.1}Se$ THIN FILMS

The response as a function of wavelength of the incident radiation was determined for the most sensitive sample using equipment in the TRW Systems Microelectronics laboratory in Redondo Beach, California. This equipment consisted of a glowbar radiation source, a self-synchronizing chopper, a Leiss monochromator, a thermocouple detector as a black detector, and a Princeton Applied Research Model HR-8 Lock-In Amplifier. The radiation from the glowbar was modulated by the chopper and dispersed in the monochromator. A slit width was used to give a resolution of approximately 0.2 microns.

To determine the spectral response of the $Pb_{0.9}Sn_{0.1}Se$ detector, it was necessary to determine the spectral distribution of the radiation incident on the detector. This was done using the thermocouple detector which was assumed to have a response which was independent of wavelength and dependent only on the energy in the incident radiation. The output of the lock-in amplifier, with the thermocouple

connected through an impedance matching transformer, was recorded at 0.2 micron intervals for wavelengths from 2 microns to 14 microns.

The sample was mounted in the second dewar which was evacuated and cooled with liquid nitrogen as before. The same bias circuitry described in the previous section was used and the chopping frequency was 1.3 kHz. The position of the dewar relative to the output aperature of the monochromator was adjusted for the best response. The detector signal indicated on the lock-in amplifier was recorded for various wavelengths of radiation and at six different temperatures. The signal voltage was then divided by the response of the thermocouple detector at the same wavelength to normalize the response to constant energy. The normalized values at each temperature were then converted to relative spectral response with a peak of unity by dividing each value by the maximum at that temperature.

C. PHOTOCONDUCTIVE TRANSIENT RESPONSE MEASUREMENT

Transient response measurements were made on $Pb_{0.9}Sn_{0.1}Se$ samples to determine the time constant of rise and decay of the detector signal when irradiated by a rectangular pulse of radiation. Since these response time constants were generally just several nanoseconds, it was imperative that the source of radiation be capable of producing a pulse with very fast rise and decay and that the equipment used to observe the detector response also have an extremely

fast response. The basic method of measurement of transient response was to irradiate the sample with a pulsed GaAs laser, photograph the response as displayed on a sampling oscilloscope, and measure the response time constants from the photograph. These constants were then compared to the calculated value of effective photoconductive lifetime.

1. Apparatus

The apparatus used for transient response measurement had three main components: the sampling oscilloscope, the cooling and bias equipment, and the laser radiation source and its pulse generating system. A schematic diagram of the circuitry in this measurement system is shown in Fig. 17 and photographs of the equipment are shown in Fig. 18.

a. Sampling Oscilloscope

The principle of operation of the sampling oscilloscope was to reconstruct one period of the waveform of a pulse train by sampling successive pulses at different points in the waveform and displaying the train of samples on the screen as in the stroboscopic effect. This made it possible for the scope to faithfully display signals with very fast rise and decay without the tremendous sacrifice of gain that generally results in conventional wide-bandwidth oscilloscopes. The oscilloscope used was a Tektronix Type 561B with a Type 3S1 dual-trace sampling unit and a Type 3T77A sampling sweep unit. It had a specified rise time

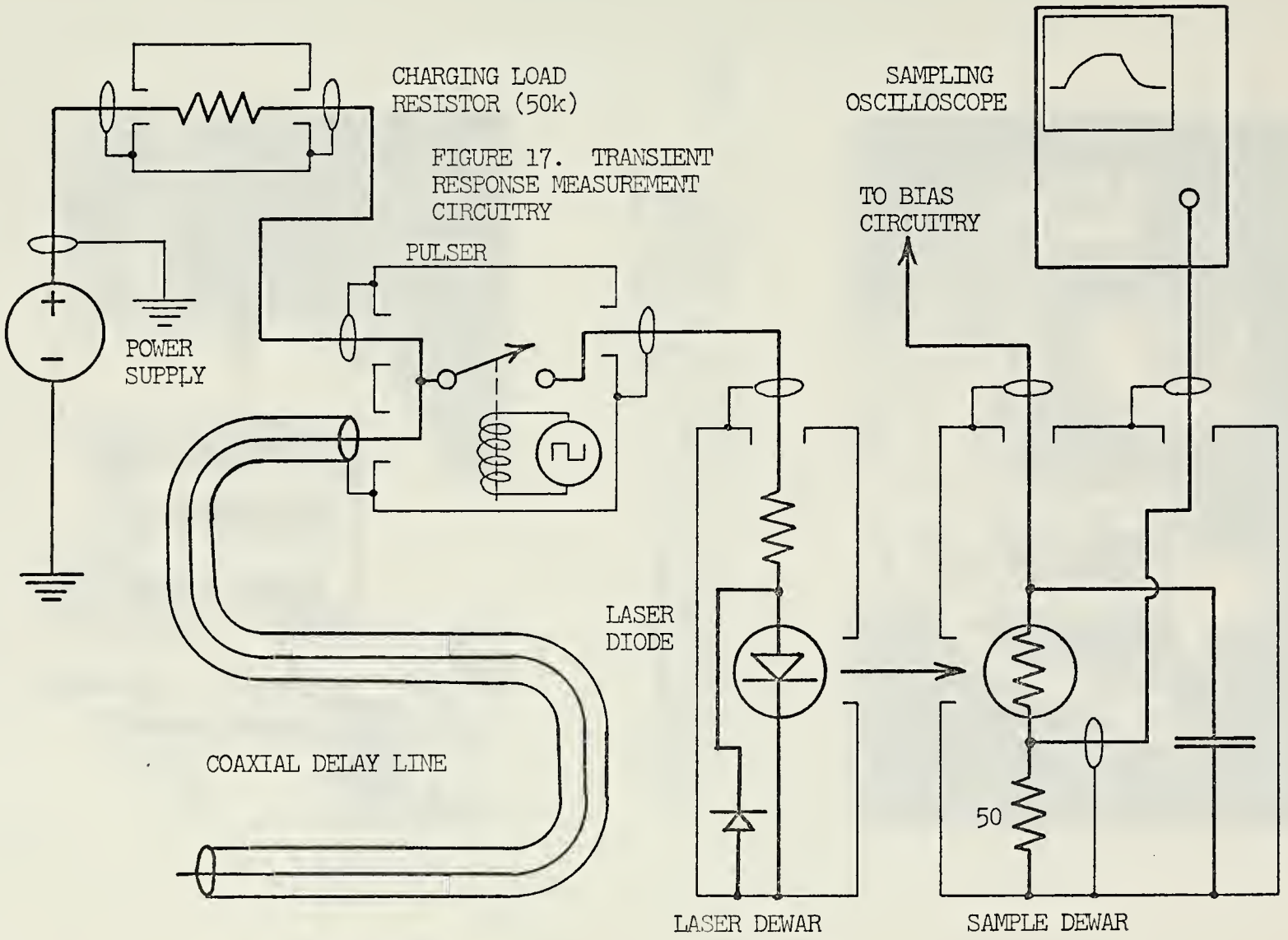

FIGURE 17. TRANSIENT RESPONSE MEASUREMENT CIRCUITRY

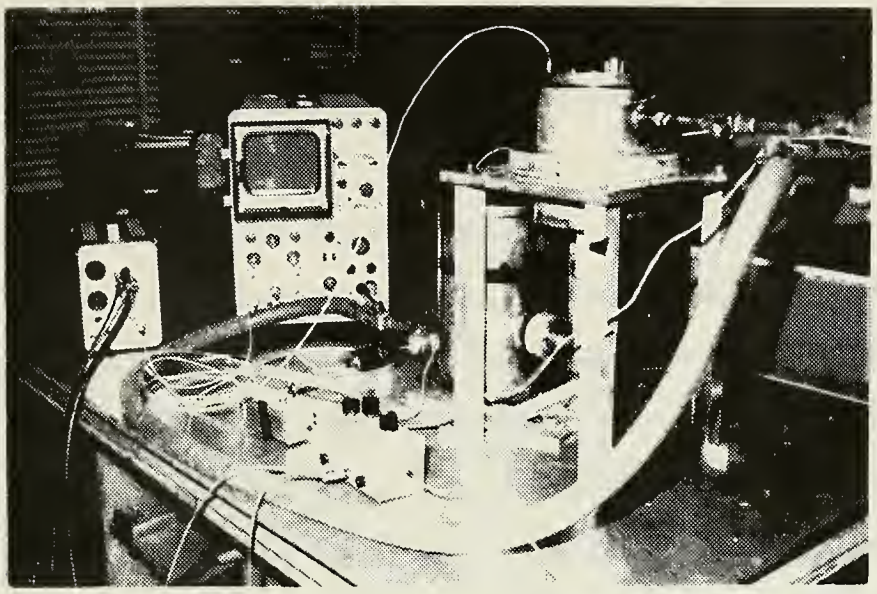

(a)

FIGURE 18. PHOTOGRAPHS OF EQUIPMENT USED FOR TRANSIENT RESPONSE MEASUREMENT: (a) PULSER AND SAMPLING OSCILLOSCOPE, (b) LASER DEWAR, SAMPLE DEWAR, AND LENS BLOCK.

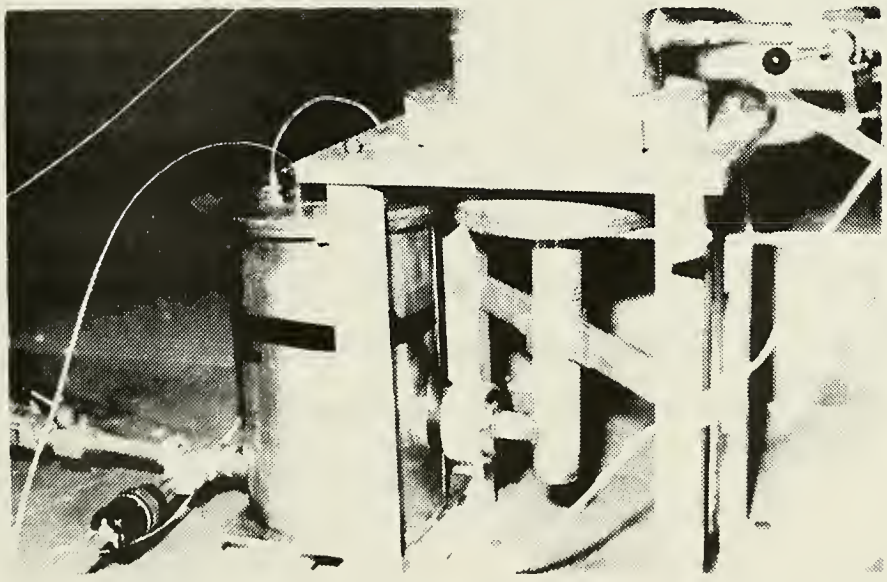

(b)

of less than 0.35 nanoseconds. The screen presentation was photographed with a Type C-27 oscilloscope camera using Polaroid 109 film.

b. Cooling and Bias Equipment

The new dewar was used to mount and cool the sample and the KRS5 window was replaced by a 125 mm focal-length f/5.0 lens. The bias circuitry was changed somewhat due to the requirements of a wide-bandwidth system. The signal was taken from a 50 ohm load resistor for impedance matching and the resistor was connected between the detector and ground in the dewar to simplify the shielding and grounding arrangement. To make the signal path as short as possible, a capacitor was connected across the sample and load resistor inside the dewar. The junction box used for blackbody response measurements was no longer required and the switch box was connected directly to the dewar (Fig. 17].

c. Laser and Pulse Generator

The laser diode used as a source of pulsed radiation was an RCE TA-7088A GaAlAs injection laser which was actually an array of fifteen heterojunction laser diodes electrically connected in series and mounted in the same package. The room-temperature operating characteristics of this device are listed below. [17]

---

[17] DeVillbiss, W. F. and Klunk, S. L., "Solid State Pulse Power Supplies for RCA GaAs Injection Lasers," RCA Optoelectronic Products Application Note AN-4469, p. 2, February, 1972.

Wavelength	9050° A
Max. pulse duration	0.2 microseconds
Max. duty factor	0.02 %
Lasing threshold current	7 A
Peak drive current	25 A
Min. peak power at 25 A. current	75 W

Since the output of the laser corresponded directly to the driving current once the lasing threshold was reached [Refs. 30 and 31), very fast rise times were possible if a current pulse of sufficient amplitude and speed of rise and decay were available. This pulse was produced using a Tektronix Model 109 pulser, which had a specified rise time of less than 0.25 nanosecond, to discharge a delay line through the laser. The pulser was basically a mechanical reed switch with mercury-wetted contacts and driven by a magnetic field oscillating at about 300 Hz. The coaxial delay line was 500 cm long, had a specified rise time of less than 0.1 nanosecond, and produced a rectangular pulse 120 nanoseconds in duration. The laser driving circuit was a 50-ohm system, and impedance matchings were required at all terminations to prevent reflections which would be detrimental to fast rise and decay. The necessity of using the 50-ohm system meant that fairly high charging voltages on the delay line were required for high injection current in the laser. Since the forward bias voltage across each of the fifteen diodes in the laswer was seven volts, at least 800 volts were required just to produce

the 7-ampere threshold current and 1500 to 2600 volts were needed for really high laser power output. This high power would have been necessary to produce an observable response from the weak samples since the sensitivity of the sampling oscilloscope was very low compared to that of the lock-in amplifier.

The laser was originally operated at room temperature with the delay line charged to 1500 volts. The voltage on a current-sampling resistor in the circuit, as observed on the sampling oscilloscope, indicated a driving current pulse of twelve to thirteen amperes which should have produced a peak power output of about thirty watts. Unfortunately, the reed switch in the pulser was only rated for 300 volts and was soon rendered inoperative by the extreme overload. Consideration was given to using a solid-state silicon-controlled-rectifier pulser since it is capable of operating at the current and voltage levels required. However, the fastest rise time of the solid-state pulsers was far too slow for this application (20 nanoseconds or more).

In order to drive the laser with the extremely fast reed switch in the pulser and still obtain fairly high peak power output from the laser, it was necessary to cool the laser using liquid nitrogen. At liquid nitrogen temperature, the threshold current and forward-biased voltages were reported to be one-tenth and one-fourth of their

room-temperature values respectively, while the radiant efficiency was reported to improve by a factor of ten [Refs. 30 and 31].

To enable operation at low temperature, the laser package was mounted on the copper cold-finger of the old dewar along with a 50-ohm matching resistor and a clipping diode. The diode was included to prevent any reverse bias of the laser due to undershoot and ringing in the power pulse which would have ruined the laser. A current sampling resistor was not included due to the difficulty in mounting the laser if its cathode had to be insulated from the cold-finger which was at ground. The KRS5 window and its mounting block on the laser dewar were replaced with a larger block holding two lenses as shown in Fig. 19. These lenses focused the light from the laser on the sample mounted in the new dewar when the two dewars were placed together as shown in Fig. 18. When the laser was cooled to around 100° K, the threshold pulse current was observed to be less than one ampere. A fairly powerful output could be obtained from the laser with only 500 volts due to the reduced forward-biased voltage and improved efficiency.

2. System Risetime Measurements

Before making any transient response measurements, the rise time and decay time of the radiation source and its power supply were determined. The photographs in Fig. 20 are the leading and trailing edges of the voltage pulse with the pulser connected directly to the sampling oscilloscope

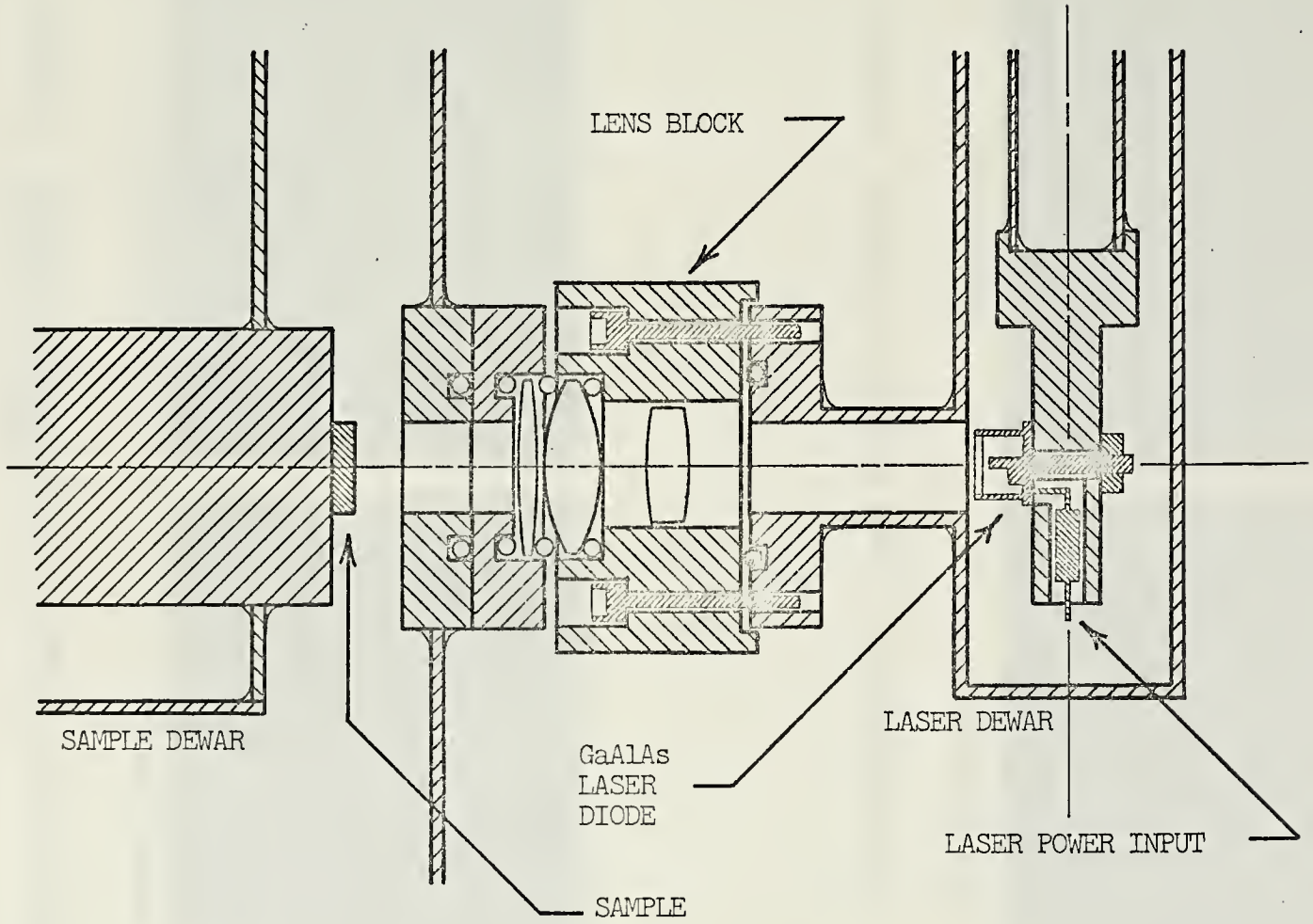

FIGURE 19. SECTIONED DRAWING OF THE OPTICAL SYSTEM USED IN TRANSIENT RESPONSE MEASUREMENTS

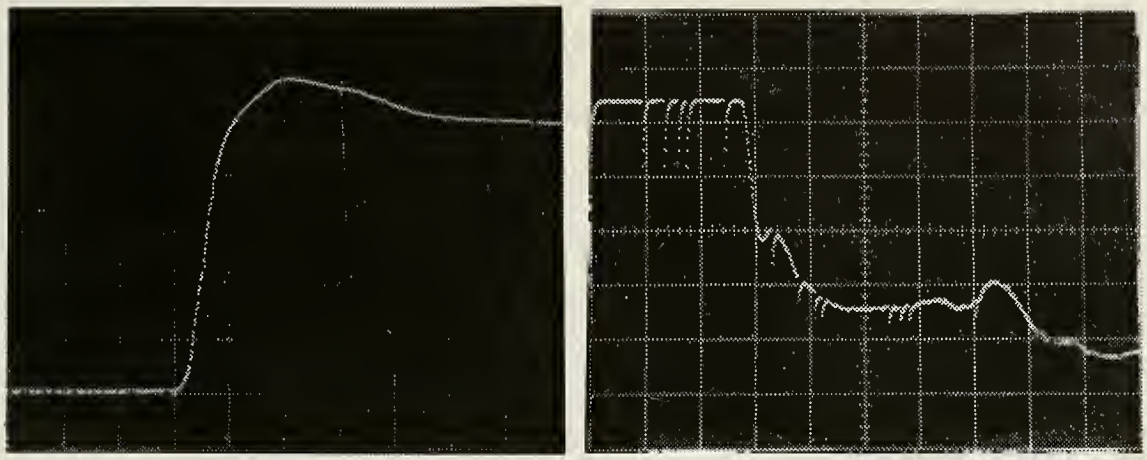

0.5 ns/division 2.0 ns/division

FIGURE 20. LEADING AND TRAILING EDGES OF THE PULSER OUTPUT

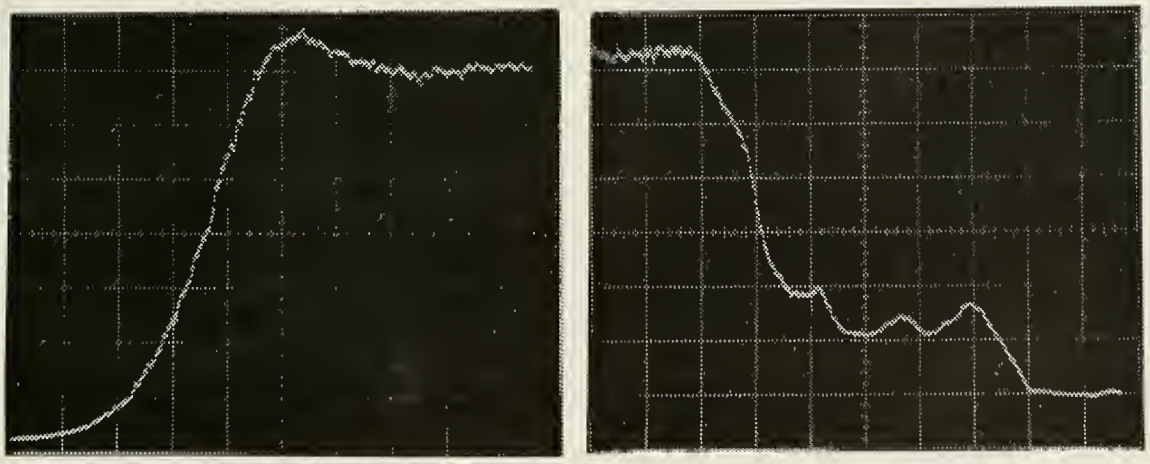

0.2 ns/division 2.0 ns/division

FIGURE 21. LEADING AND TRAILING EDGES OF THE P-I-N DIODE RESPONSE TO THE LASER OUTPUT

input through an attenuator. The ten-to-ninety percent rise and decay times of the delay line, pulser, and sampling oscilloscope together were found to be 0.3 and 2.4 nanosecond respectively, well within the required range. The lower step in the decay of the pulse was a characteristic of the pulser-delay line combination and was unavoidable. This step reduced the accuracy with which decay time constants could be measured but was not considered a serious limitation.

The form of the light pulse from the laser was observed by focusing the radiation on a fully-depleted silicon p-i-n photodiode which was reverse biased with 45 volts. The voltage produced by the diode photo-current flowing through a 50 ohm load resistor was displayed on the sampling oscilloscope. The response time of this type of photo-diode is typically around 10 picoseconds so the waveform of the output of the diode circuit was considered to be essentially the same as the waveform of the light pulse. The leading and trailing edges of the response of the p-i-n diode to the laser pulse are shown in Fig. 21. It is interesting to note how closely the laser light pulse conformed to the shape of the driving current pulse as indicated by the identical lower step in the decay portion of the waveform. The ten-to-ninety percent rise and decay times of the laser light pulse were found to be 0.5 ns and 5 ns respectively. The decay time was somewhat longer than expected. However, in view of the fact that a ninety-to-ten

percent decay time is equivalent to more than two exponential time constants, this decay was still considered quite satisfactory.

3. Transient Response Measurement Procedure

The procedure for the measurement of transient response was begun by mounting the sample on the cold-surface of the new dewar as for blackbody response measurement and evacuating both the sample dewar and the laser dewar. The two dewars were placed together as shown in Fig. 18 and both the laser and the sample were cooled to around 100° K using liquid nitrogen. The sample bias current was adjusted to a relatively higher value than that used for blackbody response to obtain a stronger output signal. With the laser power supply and pulser turned on, the trigger, vertical scale, and time scale controls on the sampling oscilloscope were adjusted for the best presentation of either the rise or decay portions of the sample response. A photograph was then taken of the scope trace using the single-sweep mode of operation. The transient response was recorded with the camera for various values of laser driving voltage at the low temperature and for various temperatures with the highest driving voltage (500 volts).

Two serious problems were encountered when the transient response measurement was attempted. The first was that the detector response on the screen was completely obscured by high frequency oscillations. These had not been evident when the p-i-n diode response was observed

because its signal was high and low sensitivity scales were used. However, they were quite strong when using the high sensitivity scales for the response of the sample. The oscillations were found to be noise transmitted by the laser pulse power supply. This problem was eliminated by replacing all leads in the pulse power supply with standard 50-ohm coaxial cable and by placing the charging load resistor in an electrically sealed enclosure.

The second problem was the large amount of attenuation of the response of the sample caused by the mismatch between the 50 ohm load resistor and the sample resistance. Even with a fairly powerful laser output and using the most sensitive vertical scale on the oscilloscope, this loss of signal made it difficult to obtain a clear presentation on the screen. This was especially troublesome when using lower laser power outputs and higher sample temperatures. The two $Pb_{0.9}Sn_{0.1}Se$ samples for which transient response measurements were made were the most sensitive of the high and low-resistance type samples. They had resistances of 9.8 k-ohms and 360 ohms and had blackbody responsivities of 81 and 0.65 volts/watt at the bias currents used respectively. Both produced approximately the same magnitude of response on the scope due to the differences in resistance matching. Transient response measurement on other less sensitive high resistance or low resistance type samples, had time permitted, would have been exceedingly difficult. The best solution to the attenuation problem was thought to

be use of a high value of load resistance and an amplifier at the sample with a high input impedance and a 50 ohm output impedance. This amplifier would be required to have a bandwidth of several hundred megahertz but only moderate or even unity gain. Time did not permit the application of this possible solution.

4. Response Time and Effective Lifetime Calculations

The rise and decay time constants were measured as exponential time constants. They were found by measuring the distances on the photographs from the start of the rise or decay to the point where the signal had risen to $(1-e^{-1})$ of its steady-state value or had fallen to e^{-1} of this value. The distances were then multiplied by the time scale. These time constants were then compared to a calculated photoconductive lifetime using the equation which was derived as follows.

First, the amplitude of the r.m.s. value of the fundamental component of the irradiating waveform from the blackbody was expressed in terms of the number of photons. The Stefan-Boltzmann relation,

$$\sigma(T_{BB}^{4} - T_{CH}^{4})$$

in the expression used for the power of the radiation signal in the blackbody response calculations was replaced with the relation,

$$\sigma' T_{BB}^{3} - \sigma' T_{CH}^{3}$$

where $\sigma' = 1.52 \times 10^{11}$ photons-sec^{-1}-cm^{-2}-°K^{-3}. This relation gave the difference in the number of photons emitted per second per unit area from the blackbody source and from the chopper blade.[18] Since only the photons which have a quantum energy greater than the energy gap in the detector material generated excess free carriers, a correction to this number was applied. The energy gap was calculated as 0.092 eV for the sample temperature of 100° K using the empirical relation found by Kim [Ref. 32], based on optical absorption data.

$$E_g(y,T) = 0.13 + 5 \times 10^{-4} T - 0.88y$$

In this relation, y is the allow percentage of SnSe content (0.1) and T is the absolute temperature. This energy gap corresponds to a cut-off wavelength of 13.5 microns. The correction factors were found from the blackbody radiation tables published by Lowan and Blanch [Ref. 33] using this wavelength and the blackbody and chopper temperatures (500° K and 300° K). These factors, $R(\lambda_{co}T_{BB})$ and $R(\lambda_{co}T_{CH})$, are simply the ratio of the number of photons with a wavelength

---

[18] Hudson, R.D., Infrared Systems Engineering, p. 21, Wiley, 1969.

less than the argument wavelength to the total number of photons for a blackbody at the argument temperature. Using these factors, the expression for the radiation signal in terms of the number of photons was written as the following.

$$N_{ph} = \alpha_{CH} \cdot \alpha_W \cdot \varepsilon_B \cdot \frac{\sigma' [R(\lambda_{co} T_{BB}) \cdot T_{BB}^3 - R(\lambda_{co} T_{CH}) \cdot T_{CH}^3]}{\pi} \cdot A_B \cdot \frac{A_D}{d^2}$$

where all the additional parameters are the same as described for the blackbody response calculations. Because of reflection from the surface of the sample, only a fraction of these photons actually entered the crystal where it was assumed they all generated a single free hole-electron pair. Therefore, applying a correction for the reflectance of the material based on the index of refraction, the rate of generation of free hole-electron pairs was written as:

$$F = \left[1 - \frac{(n-1)^2}{(n+1)^2}\right] \cdot N_{ph}$$

where n is the index of refraction which is approximately five for lead-tin selenide.

The expression for the photo-generated current was shown in Chapter II to be the following.

$$I_{ph} = eF \frac{V}{L^2} (\tau_e \mu_e + \tau_h \mu_h)$$

Since lead-tin selenide is an intrinsic photoconductive material, the hole and electron lifetimes can be considered

to be equal. Expressing the majority carrier drift mobility as μ and the mobility ratio as b, the above expression can be written as

$$I_{ph} = eF \frac{V}{L^2} \mu \tau r_b$$

In this expression,

$r_b = (1 + \frac{1}{b})$ for n-type material and

$r_b = (b + 1)$ for p-type material.

$b = \mu_e/\mu_h$

The expression for the photo-current may be rewritten as the following.

$$I_{ph} = \frac{V_{ph}}{R} = eF \frac{I_o R}{L^2} \mu \tau r_b$$

Solving this expression for τ gives an expression for effective excess carrier lifetime in terms of the measurement constants, the sample resistance (R), electrical properties, and the response voltage (V_{ph}).

$$\tau = \frac{V_{ph} L^2}{eF\mu r_b I_o R^2}$$

Using this expression, an effective excess carrier lifetime was calculated for the two samples for which transient

response measurements were made. It must be emphasized that these values were only considered as very rough estimates of lifetime since there were two major sources of uncertainty. First, the Hall mobility was used for the majority carrier drift mobility. Although the difference between the two, which depends on the type of scattering and other factors, is usually not large, the two are definitely not the same. The second source of error was in the mobility ratios which were not known for the samples measured. This number has generally been observed to be in the range from three to ten and a value of five was used. Although the uncertainty due to the mobility ratio did not have a large effect in the effective lifetime for the n-type sample (OB-12-3), it was of considerable significance in the calculation for the p-type sample (OB-10-4).

V. RESULTS AND DISCUSSION

A. RESPONSIVITY AND DETECTIVITY

Blackbody (500° K) detector measurements were made on fifteen $Pb_{0.9}Sn_{0.1}Se$ thin-film samples. The signal and normalized noise voltages, their ratio, the noise equivalent power, and the detectivity and responsivity at an optimum value of bias current selected for best signal-to-noise ratio are listed in Table V. The crystal structure, thickness, electrical properties, and photoconductive performance of the samples are listed in Table IV.

It was found that the sensitivity of the samples as indicated by the responsivity was not dependent upon the carrier concentration in any significant way. However, a fairly good correlation between the photo-sensitivity and the type of crystal structure of the sample was observed. The most sensitive samples were single-crystal with (100) orientation. Samples with any (111)-oriented crystal structure had much lower sensitivities. Before an explanation for such dependence is attempted, it should be noted that the observed trend had a few obvious discrepancies. According to the criteria given, samples OB-13-2 and OB-13-4 which were polycrystalline (111) + (100) should have had poor sensitivity and sample OB-11-5 which was single-crystal (100) should have had good sensitivity. However, this was not the case. The following discussion will include these exceptions as well.

TABLE IV

SUMMARY OF PHOTOCONDUCTIVE PERFORMANCE OF $Pb_{0.9}Sn_{0.1}Se$ SAMPLES

Sample Number	Crystal Structure	Thickness (microns)	Carrier Concentration ($1/cm^3$)	Hall Mobility ($cm^2/V\text{-}sec$)	Resistance 300°K/100°K (k-ohm)	Detectivity ($cm/Hz^{1/2}W$)	Responsivity (V/W)
OB-7-3	PC(100)+(111)	2.18	$1.48x10^{17}$(p)	1040	.70/.76	$7.1x10^5$	0.45
OB-7-4	PC(100)+(111)	2.18	$1.30x10^{17}$(p)	4230	.66/.27	$2.3x10^5$	0.034
OB-8-3	PC(100)+(111)	2.66	$7.82x10^{16}$(p)	6210	.68/.20	$2.3x10^5$	0.045
OB-8-4	PC(100)+(111)	2.75	$6.43x10^{16}$(p)	7350	.72/.25	$1.0x10^6$	0.11
OB-10-2	SC(100)	0.95	$5.66x10^{17}$(p)	77.0	.9 /8.2	$2.0x10^6$	3.8
OB-10-3	SC(100)	0.95	$1.06x10^{17}$(p)	468	2.6 /6.4	$1.1x10^7$	18.0
OB-10-4	SC(100)	0.99	$1.11x10^{17}$(p)	504	4.0 /9.8	$7.2x10^6$	61.0
OB-11-2	SC(100)	1.93	$4.90x10^{16}$(p)	139	1.7 /20.5	$7.9x10^6$	23.0
OB-11-3	SC(100)	2.02	$5.14x10^{16}$(p)	134	1.6 /16.0	$4.0x10^6$	23.0
OB-11-5	SC(100)	2.00	$4.73x10^{17}$(n)	1600	.32/.13	$6.9x10^5$	0.09
OB-12-3	SC(111)	1.13	$5.42x10^{17}$(n)	857	1.3/.36	$4.9x10^6$	0.65

TABLE IV (cont)

SUMMARY OF PHOTOCONDUCTIVE PERFORMANCE OF $Pb_{0.9}Sn_{0.1}Se$ SAMPLES

Sample Number	Crystal Structure	Thickness (microns)	Carrier Concentration ($1/cm^3$)	Hall Mobility ($cm^2/V\text{-}sec$)	Resistance 300°K/100°K (K-ohm)	Detectivity ($cm/Hz^{1/2}W$)	Responsivity (V/W)
OB-12-5	SC(111)	.93	2.29×10^{17}(p)	29200	1.0/ .2	1.2×10^5	0.035
OB-13-2	PC(100)+(111)	.80	1.56×10^{18}(p)	22.0	8.0/12.5	3.1×10^5	2.5
OB-13-4	PC(100)+(111)	.87	3.75×10^{17}(p)	27.7	7.5/17.0	1.3×10^6	5.8
K-5-3	PC(100)+(111)	3.40	4.83×10^{17}(p)	1450	.300/.106	7.8×10^4	0.003

The crystal type and orientation were generally determined by X-ray diffraction analysis for only one sample from each deposition batch. The assumption was made that all samples from the same deposition (indicated by the first number in the sample identification) had essentially the same crystal structure. It is possible, however, that this assumption was not always valid. A sample listed as single-crystal (100) such as OB-11-5, for example, may actually have had some (111) components present. One listed as polycrystalline (111) + (100) such as OB-13-2 and OB-13-4 may have had very little of the (111) crystal present. In the case of the OB-13 batch, the X-ray diffractometer tracing indicated a definite presence of some (111)-oriented crystal together with the strong (100) component. However, the absence of any rings in the Laue photographs indicated that the film was single-crystalline. The deposition parameters used for the batch were close to those which have produced single-crystal (100) in other depositions [Ref. 1].

Some support was lent to this hypothesis by the values of low-temperature Hall mobilities and the changes in resistance of the samples from room temperature to 100° K as listed in Table IV. All of the samples listed as single-crystal (100), except OB-11-5, had low mobilities and showed an increase in resistance of as much as an order of magnitude from the room-temperature value to the value at 100° K, such as in samples OB-11-2 and OB-11-3. Both samples listed as

TABLE V

MEASUREMENT DATA TAKEN FOR 500° K BLACKBODY RESPONSE EVALUATION OF $Pb_{0.9}Sn_{0.1}Se$ SAMPLES

Sample Number	Bias Current (mA)	Signal Voltage (uV)	Normalized Noise Voltage (uV/Hz$^{1/2}$)	Signal To Noise Ratio	Noise Equiv. Power (uW)	Detectivity (cm^2/Hz$^{1/2}$W)	Responsivity (V/W)
OB-7-3 (1)	10.0	2.8	2.8	1.0	6.3	7.1×10^5	0.45
OB-7-4 (1)	10.0	.21	.066	3.2	1.9	2.3×10^5	0.034
OB-8-3 (1)	15.0	.28	.089	3.2	2.0	2.3×10^5	0.045
OB-8-4 (1)	20.0	.68	.046	15.0	.43	1.0×10^6	0.11
OB-10-2(2)	1.5	275	.87	320	.23	2.0×10^6	3.8
OB-10-3(2)	.75	1300	.73	1700	.042	1.1×10^7	18.0
OB-10-4(1)	2.0	380	3.8	100	.062	7.2×10^6	61.0
OB-11-2(1)	1.5	140	1.3	110	.57	7.9×10^6	23.0
OB-11-3(1)	2.0	140	2.6	56.	1.1	4.0×10^6	23.0
OB-11-5(2)	10.5	6.5	.058	112.	.64	6.9×10^5	0.09
OB-12-3(2)	9.0	43.0	.056	770	.092	4.9×10^6	0.65
OB-12-5(2)	14.0	2.5	.13	19.	3.7	1.2×10^5	0.035

(1) indicates sample measured in dewar #1, (2) indicates sample measured in dewar #2

TABLE V (cont.)

MEASUREMENT DATA TAKEN FOR 500° K BLACKBODY RESPONSE EVALUATION OF $Pb_{0.9}Sn_{0.1}Se$ SAMPLES

Sample Number	Bias Current (uA)	Signal Voltage (uV)	Normalized Noise Voltage ($uV/Hz^{1/2}$)	Signal To Noise Ratio	Noise Equiv. Power (uW)	Detectivity ($cm^2/Hz^{1/2}W$)	Responsivity (V/W)
OB-13-2 (2)	10.0	190	3.6	55.0	1.5	$3.1x10^5$	2.5
OB-13-4 (2)	7.0	415	2.0	206.0	.35	$1.3x10^6$	5.8
K-5-3 (2)	14.0	.23	.018	13.0	5.7	$7.8x10^4$	0.003

single-crystal (111), OB-12-3 and OB-12-5, on the other hand, had high mobilities and showed a strong decrease in resistance with decreasing temperature. High mobility and a variation of resistance proportional to temperature were considered as characteristic of samples with (111) crystal orientation, and low mobility and an inverse resistance variation with temperature as characteristic of samples with (100) orientation. This supported the supposition that there was actually some (111) crystal present in OB-11-5 and very little (111) in OB-13-2 and OB-13-4.

Using this approach to explain the three major discrepancies, it appeared that single-crystal (100) orientation in the material was a definite prerequisite for high sensitivity in the $Pb_{0.9}Sn_{0.1}Se$ thin films. The reason for this is not clearly understood. It has been proposed that the growth of crystal structure with (100) orientation on the CaF_2 substrates, which were (111) oriented, created some crystal defects. The low mobility found in the single-crystal (100) films possibly was caused by these defects. If these defects acted as trapping centers, according to the minority carrier trapping model described in Chapter II, the additional traps would help to increase the lifetime of the majority carriers and thereby increase the sensitivity. Therefore, it was thought that the crystal orientation mismatch between the film and substrate was the primary reason for the higher sensitivities in single-crystal (100) films.

The responsivities which were measured in the $Pb_{0.9}Sn_{0.1}Se$ samples ranged from 0.003 volts per watt to 61 volts per watt, which is quite high compared with the best 500° K blackbody responsivity of PbSnTe photovoltaic detectors of around 100 to 125 volts per watt. The detectivity varied from high-10^4 to low-10^7 ($cm\text{-}Hz^{-1/2}\text{-}W^{-1}$). These values of detectivity were all very low compared to the theoretical background-limited value and to the detectivities of other infrared detectors. The primary reason for the low detectivity was the relatively large amounts of noise measured from the samples. The magnitude of the noise seemed to vary directly as the sensitivity which tended to restrict all the detectivities to a relatively smaller range. The reason for the correspondence of noise and sensitivity is not known. The primary source of noise was thought to be the contacts on the thin films. The difference in the work function of the gold and semiconductor [Ref. 34] resulted in the formation of a weak metal-semiconductor diode at their junction. When potential was applied across the sample, one of the two diodes became reverse biased and breakdown occurred when current flowed through the junction causing a large amount of noise.[19] In addition, the silver-epoxy used to bond the wires to the gold pads probably was a strong source of noise. Data was taken to plot a noise power frequency spectrum for the sample which had the most noise,

---

[19] Rose, A., Concepts in Photoconductivity and Allied Problems, p. 99, Wiley, 1963.

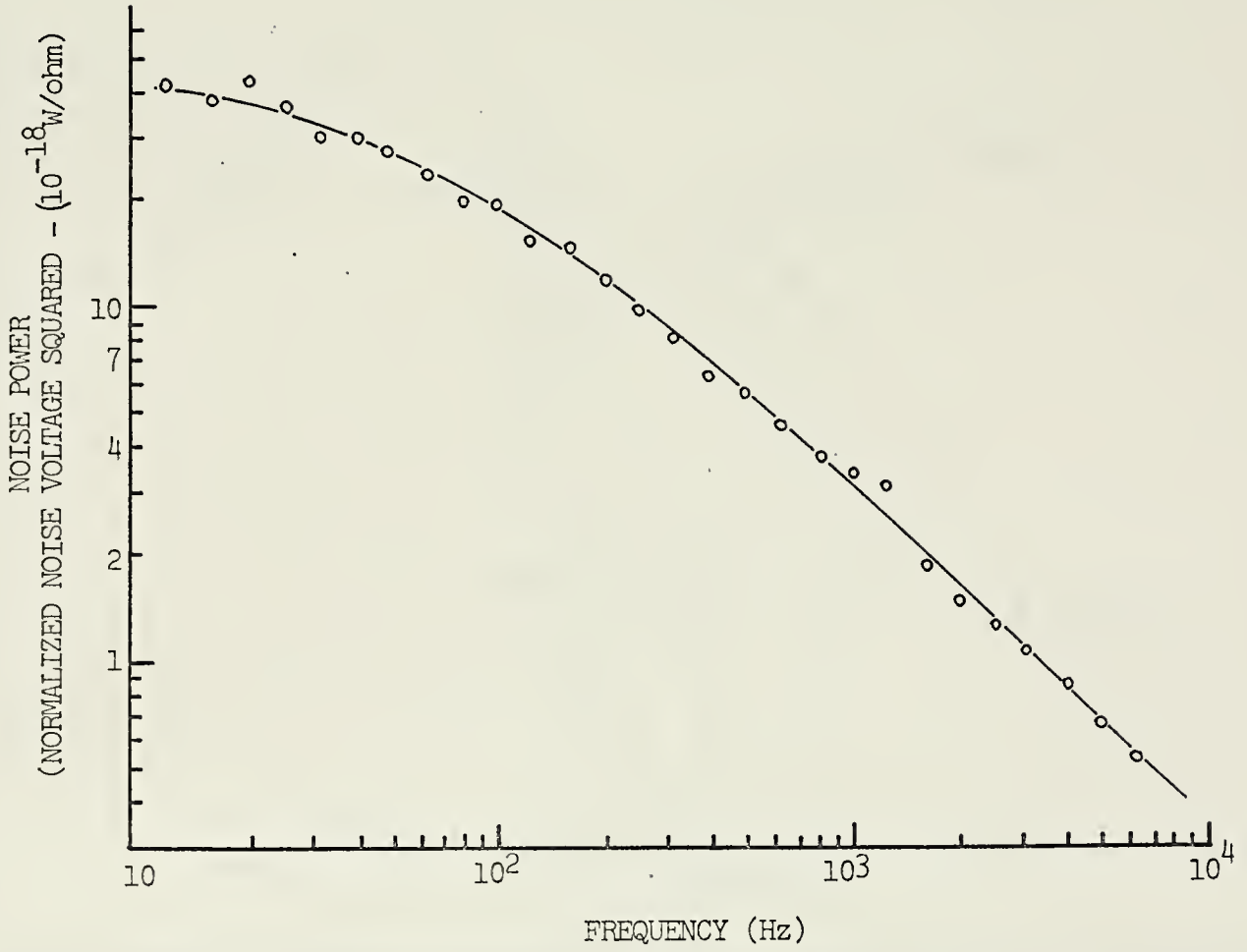

FIGURE 22. NOISE POWER SPECTRUM FOR SAMPLE OB-10-4

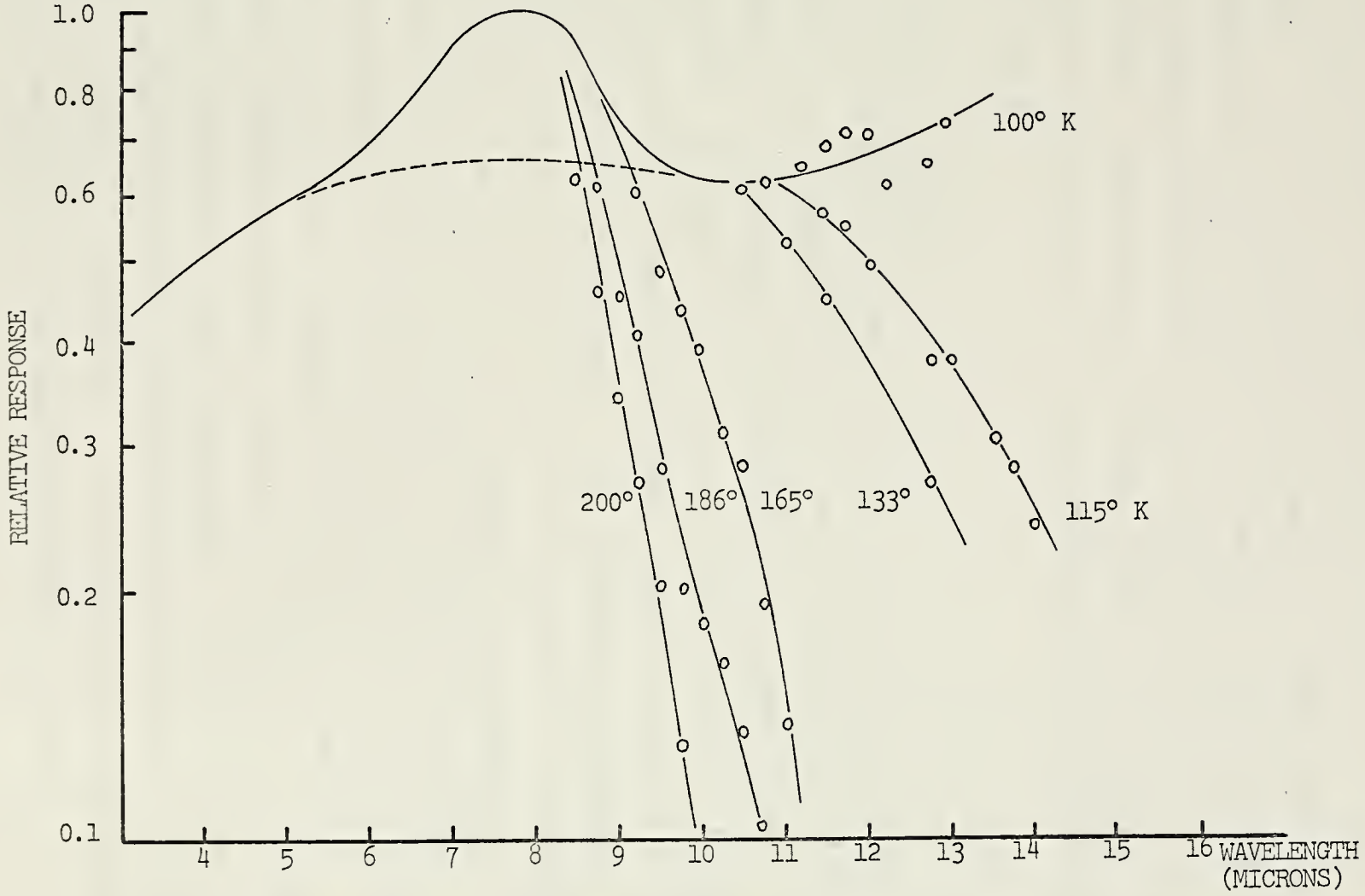

FIGURE 23. RELATIVE SPECTRAL RESPONSE OF SAMPLE OB-10-4 AT SIX DIFFERENT TEMPERATURES

OB-10-4. As shown in Fig. 22, the spectrum had the form of 1/f noise which is the type generally associated with contacts. At the measurement frequency of 1 kHz, the noise was dominated by this type and considerably higher measurement frequencies would have been required to get out of the 1/f region. Better means of making contact to the semiconductor seem necessary to reduce the noise to considerably lower levels.

B. SPECTRAL RESPONSE

The data taken on sample OB-10-4 for spectral response at each of six temperatures was normalized to unity at the wavelength of the highest response for each temperature and plotted as shown in Fig. 23. The only puzzling feature of the spectral response is the peak response shown at 7.5 microns for each temperature. Such temperature-invariance strongly suggest that this peak was the result of experimental measurement problems and not a property of the material. The peak was thought to have been the result of a dip in the response of the thermocouple detector used for calibration of the source. An accurate measurement of spectral response requires that the calibrating detector have a flat response independent of the wavelength. The particular thermocouple detector in the TRW Systems set up was used only for detector measurement in the visible and near infrared regions and had not been calibrated beyond 5 microns.

When this peak at 7.5 microns was disregarded, as shown by the dotted line in Fig. 23, the spectral response and its variation with temperature were very close to what was expected. The cut-off or photoconductive threshold wavelength for each temperature was defined as the wavelength at which the response had fallen to 0.707 of its peak value. The peak value was considered as about 0.64 when the artificial peak at 7.5 microns was disregarded. The photon energies for these cut-off wavelengths were considered to be the energy gap of the material and were plotted versus the temperature in Fig. 24. The line drawn on this graph represents the values of absorption edge given by the empirical relation derived by Kim [Ref. 32] based on optical measurements.

$$E_g(y,T) = 0.13 + 5.0 \times 10^{-4}T - 0.88y(eV)$$

There is very good agreement between the values of energy gap found by spectral response measurement and those predicted by the relation given above. This indicates that the $Pb_{0.9}Sn_{0.1}Se$ thin film was a true intrinsic photoconductor in that the only significant electron optical excitation process was from the valence band to the conduction band.

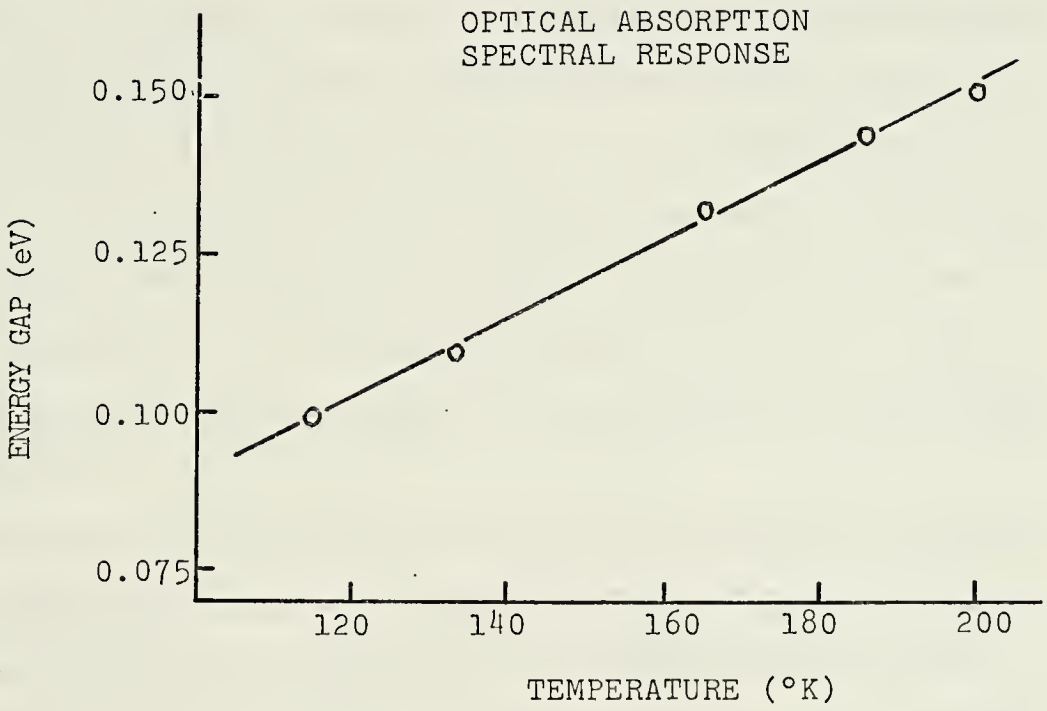

FIGURE 24. VARIATION OF ENERGY GAP WITH TEMPERATURE IN $Pb_{0.9}Sn_{0.1}Se$ AS INDICATED BY OPTICAL ABSORPTION [REF. 32] AND SPECTRAL RESPONSE.

C. PHOTOCONDUCTIVE TRANSIENT RESPONSE

Due to time limitations and the attenuation problem discussed in Chapter III, photoconductive transient response measurements were made only on two samples, the most sensitive high-resistance sample, OB-10-4, and the most sensitive low-resistance sample, OB-12-3. The rise and decay times for both samples are longer than the calculated effective lifetimes. This is consistent with the model based on fast trapping of minority carriers which prevented recombination from occurring at a faster rate. The reason for the difference between the rise and decay time constants for both samples is not known. This difference indicates that there are probably some complex transition processes not taken into consideration in the highly simplified model. These rise and decay time constants at low temperature are listed in Table VI.

The decay time constants which were measured for different temperatures and for different values of laser driving voltage are listed for each sample in Tables VII and VIII. There is not much variation in the decay time with the laser power which may be considered to indicate that saturation of the traps did not occur at this level of radiation intensity. The variation of relaxation time with temperature which was observed in sample OB-12-3 is consistent with the

TABLE VI. RISE AND DECAY TIME CONSTANTS AND CALCULATED EFFECTIVE LIFETIME AT 100° K

Sample Number	Rise Time (ns)	Decay Time (ns)	Calc. Lifetime (ns)
OB-10-4	10.	48.	3.4
OB-12-3	6.0	25.	1.9

TABLE VII. DECAY TIME CONSTANTS MEASURED WITH FOUR VALUES OF LASER POWER AT 100° K.

Laser Driving Voltage	Decay Time Constants (ns)	
	OB-10-4	OB-12-3
500	48.	25.
400	48.	22.
300	44.	22.
200	40.	20.

TABLE VIII. DECAY TIME CONSTANTS MEASURED AT VARIOUS SAMPLE TEMPERATURES (Laser voltage = 500 volts)

OB-10-4		OB-12-3	
Temperature (° K)	Decay Time (ns)	Temperature (° K)	Decay Time (ns)
98	48.	98	25.
120	48.	112	24.
135	60.	121	25.
153	64.	131	22.
173	68.	142	17.

trapping model.[20] According to this model, higher temperatures increase the probability that a trapped carrier may be excited into the conduction band by lattice thermal energy. This decreases the number of trapped carriers which results in an increase in the rate of recombination. The variation of relaxation time with temperature in sample OB-10-4, however, is contradictory to this explanation in that the relaxation time was observed to increase fairly significantly with increasing temperature. There was not enough data taken to indicate an explanation for this departure from the model.

---

[20] Klaassen, F. M., and others, "On the Temperature Dependence of the Photoconductive Decay Time of Films of the Lead Salts," Physica, v. 26, p. 625, August, 1960.

VI. SUMMARY

Photoconductivity has been developed in $Pb_{0.9}Sn_{0.1}Se$ thin films. Used as infrared detectors, blackbody responsivities up to 61 volts per watt at 100° K have been obtained. This is the highest value reported for this narrow-gap semiconductor alloy. It approaches the best reported value of 100 to 125 volts per watt in the $Pb_{1-x}Sn_xTe$ photovoltaic detectors which became commercially available in the past year or so.

Blackbody response measurements were made on fifteen $Pb_{0.9}Sn_{0.1}Se$ thin-film samples, the spectral response of the most sensitive sample was measured, and transient response measurements were made on two representative samples. The following four major conclusions were made based on this research: 1) $Pb_{0.9}Sn_{0.1}Se$ thin films which have single-crystal (100)-oriented structure are much more sensitive than films which have a significant amount of (111)-oriented structure present. 2) The detectivities measured were limited to low values due to high detector noise thought to be primarily caused by the electrical contacts. 3) The $Pb_{0.9}Sn_{0.1}Se$ films are intrinsic photoconductors in which the fundamental electron optical excitation process is from the valence band to the conduction band and in which the energy gap is a linear function of temperature. 3) The minority carrier trapping model is partially

applicable to $Pb_{0.9}Sn_{0.1}Se$. However, a considerable amount of research needs to be done in the area of the photoconductive transient response before the energy transition processes are well understood.

APPENDIX A

This section is the derivation of the error factor which is present when a noise signal with Gaussian amplitude distribution is measured using a full-wave rectifier and an average-reading meter which has been scaled to indicate the r.m.s. value of a sine wave. The Gaussian distribution function of a random voltage v with a zero average value and an r.m.s. value of σ (standard deviation in the distribution function) is the following:

$$P(v) = \frac{1}{2\pi\ \sigma}\ e^{-v^2/2\sigma^2} \qquad -\infty \leq v \leq \infty$$

When this signal is full-wave rectified, the probability of a negative value of v becomes zero and the probability of any positive value is doubled (since the area under the probability distribution curve must remain unity). The distribution function of the full-wave rectified signal is then the expression below.

$$P(v)_{FWR} = \frac{2}{\sqrt{2\pi}\ \sigma}\ e^{-v^2/2\sigma^2} = \sqrt{\frac{2}{\pi}}\ \frac{1}{\sigma}\ e^{-v^2/2\sigma^2}$$

The meter will then respond to the average value of this random signal, which, if the process is assumed to be ergodic, can be assumed to be the statistical mean or expected value. This is found by performing the following integration

$$E(P(v)_{FWR}) = \int_{-\infty}^{\infty} vP(v)_{FWR}\, dv$$

$$= \frac{1}{\sigma}\sqrt{\frac{2}{\pi}} \int_{o}^{\infty} ve^{-v^2/2\sigma^2}\, dv$$

$$u = \frac{v^2}{2\sigma^2} \qquad du = \frac{v}{\sigma^2}\, dv \qquad vdv = \sigma^2\, du$$

$$E(P(v)_{FWR}) = \sqrt{\frac{2}{\pi}}\, \sigma \int_{o}^{\infty} e^{-u} du = \sqrt{\frac{2}{\pi}}\, \sigma$$

Therefore, a direct average-reading meter with no scaling would only indicate $\sqrt{2/\pi}\sigma$ or about 0.798σ. If the meter is scaled to indicate the r.m.s. value of a sine wave, as on the PAR Lock-In Amplifier, the meter automatically multiplies the actual reading by the ratio of the r.m.s. value of a sine wave ($1/\sqrt{2}$ times the peak value) to the average value ($2/\pi$ times the peak value). The built-in scaling factor is then the following.

$$\frac{1/\sqrt{2}}{2/\pi} = \frac{\pi}{2\sqrt{2}}$$

The scaled meter will then indicate

$$\frac{\pi}{2\sqrt{2}} \cdot \sqrt{\frac{2}{\pi}} \cdot \sigma = \frac{\sqrt{\pi}}{2}\, \sigma \doteq .886\, \sigma$$

Since the correct r.m.s. value of the noise signal is σ, the meter indication must be multiplied by

$$\frac{2}{\sqrt{\pi}} = 1.128$$

which is the correction factor which was used when necessary.

APPENDIX B

This section is the derivation of the correction factor required due to the signal loss in the load resistor when

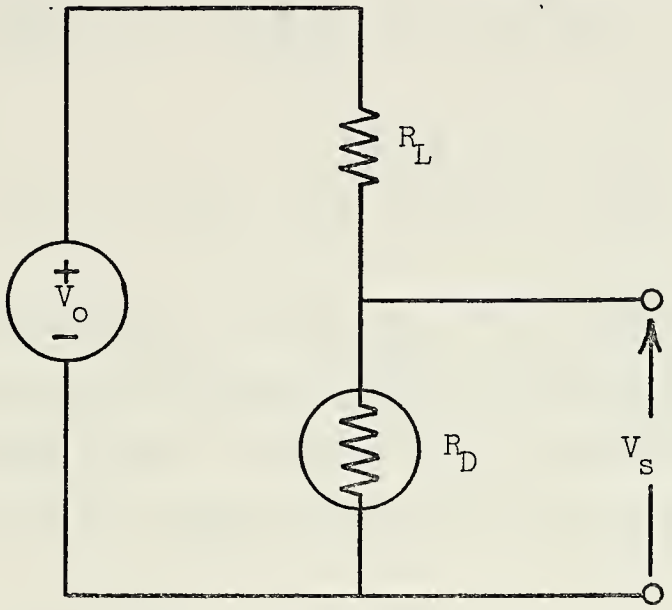

FIGURE 25. SIMPLIFIED DETECTOR CIRCUIT

blackbody response was measured. For the circuit above, the change in the output voltage V_S is the measured detector signal. To find how this is influenced by the change in the detector resistance, which is the true photoconductivity signal, and by the load resistor, the following derivative is taken.

$$V_S = \frac{R_D}{R_L + R_D} V_o$$

$$\frac{dV_S}{dR_D} = \left(\frac{1}{R_L + R_D} - \frac{R_D}{(R_L + R_D)2}\right) V_o$$

The bias current is

$$I_o = \frac{V_o}{R_L + R_D}$$

$$\frac{dV_S}{dR_D} = \left[1 - \frac{R_D}{R_L + R_D}\right] I_o = \frac{R_L}{R_L + R_D} \; I_o$$

$$v_{pc} = I_o \, dR_D = dV_S\left[\frac{R_L + R_D}{R_L}\right] = dV_S\left(1 + \frac{R_D}{R_L}\right)$$

The true photoconductivity voltage v_{pc}, which would result if the ideal case of an invariant bias current or infinite load resistance were used, can therefore be obtained by multiplying the output signal by the following factor.

$$\left(1 + \frac{R_D}{R_L}\right)$$

APPENDIX C

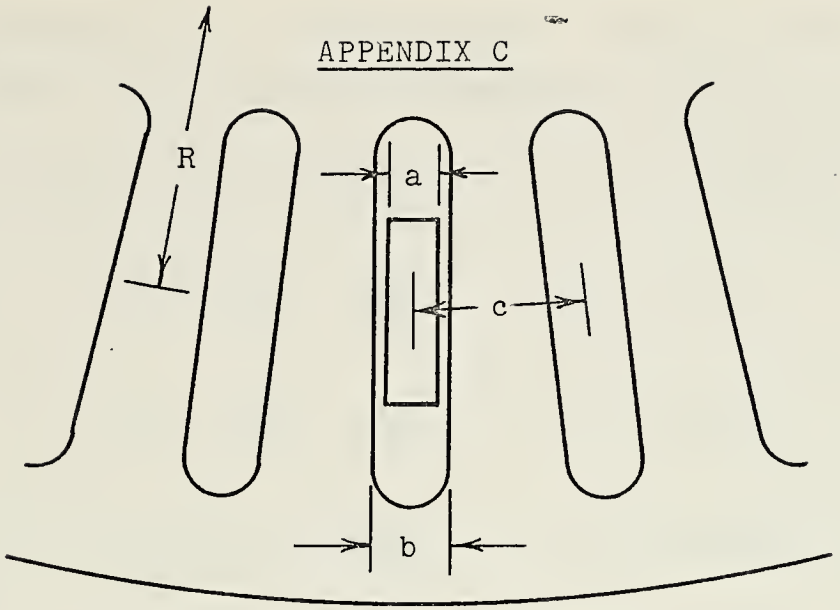

FIGURE 26. SCALE DRAWING OF THE CHOPPER BLADE AND BLACKBODY SOURCE APERATURE (TWICE ACTUAL SIZE)

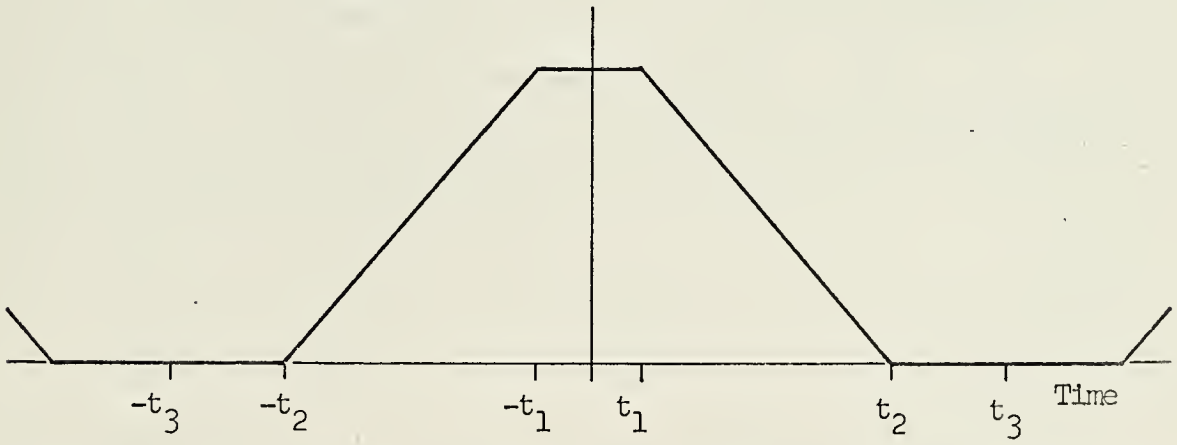

FIGURE 27. TIME WAVEFORM OF THE MODULATED BLACKBODY RADIATION

This section is an explanation of the method used to find the form factor correction for the chopping waveform of this particular radiation modulation arrangement. This form factor is simply the ratio of the r.m.s. value of the fundamental component of the waveform to the peak-to-peak value. The drawing in Fig. 26 is a scale representation

of the blackbody source aperature and a sector of the chopper blade. Based on this geometry, the time points in the radiation waveform in Fig. 27 are the following:

$$t_1 = \frac{b-a}{2} \cdot \frac{1}{2\pi RS} \qquad a = .32 \text{ cm}$$

$$t_2 = \frac{b+a}{2} \cdot \frac{1}{2\pi RS} \qquad b = .45 \text{ cm}$$

$$t_3 = c/2 \cdot \frac{1}{2\pi RS} \qquad c = 1.07 \text{ cm}$$

Here, S is the chopper blade speed in revolutions per second. Using these time points, a numerical Fourier integration of the waveform was performed. The r.m.s. value of the fundamental component was found to be 0.375 times the peak-to-peak value.

LIST OF REFERENCES

1. McBride, W. G., Thin-Film $Pb_{0.9}Sn_{0.1}Se$ Photoconductive Infrared Detectors: Part I Metallurgical and Electrical Measurements, M.S. Thesis, U.S. Naval Postgraduate School, 1972.

2. Brebrick, R. F. and Allgaier, R.S., "Composition Limits of Stability of PbTe," Journal of Chemical Physics, v. 32, p. 1826-1831, June, 1965.

3. Melngailis, I. and Harmon, T. C., "Simple Crystal Lead-Tin Chalcogenides," Semiconductors and Semimetals: Infrared Detectors, v. 5, p. 111-174, Academic Press, 1970.

4. Strauss, A. J., "Metallurgical and Electronic Properties of $Pb_{1-x}Sn_xTe$ and $Pb_{1-x}Sn_xSe$, and Other IV-VI Alloys," Transactions of the Metallurgical Society of the AIME, v. 242, p. 354-365, March 1968.

5. Calawa, A. R., and others, "Crystal Growth, Annealing, and Diffusion of Lead-Tin Chalcogenides," Transactions of the Metallurgical Society of the AIME, v. 242, p. 374-383, March 1968.

6. Dimmock, J. O., Melngailis, I. and Strauss, A. J.,"Band Structure and Laser Action in $Pb_xSn_{1-x}Te$," Physical Review Letters, v. 16, p. 1193-1196, June 27, 1966.

7. Strauss, A. J., "Inversion of Conduction and Valence Bands in $Pb_{1-x}Sn_xSe$ Alloys," Physical Review, v. 157, p. 608-611, 15 May 1967.

8. Harmon, T. C., and others, "Temperature and Compositional Dependence of Laser Emission in $Pb_{1-x}Sn_xSe$," Applied Physics Letters, v. 14, p. 333-334, 1 June 1969.

9. Wang, C. C., Properties of Thin Film $Pb_{1-x}Sn_xTe$ and $Pb_{1-y}Sn_ySe$ Infrared Photoconductors, Ph.D. Thesis, University of California, Los Angeles, 1971.

10. Hoff, G. F., Band Inversion and Electrical Properties of Lead-Tin Selenide Semiconducting Alloys, Ph.D. Thesis, University of Maryland, 1970.

11. Putley, E. N., The Hall Effect and Related Phenomena, Butterworths, 1960.

12. Rose, A., Concepts in Photoconductivity and Allied Problems, Wiley, 1963.

13. Rose, A., "Performance of Photoconductors," Photoconductivity Conference, p. 3-48, Wiley, 1956.

14. Rittner, E. J., "Election Processes in Photoconductors," Photoconductivity Conference, p. 215-268, Wiley, 1956.

15. Bube, R. H., Photoconductivity in Solids, Wiley, 1962.

16. Stöckmann, F., "Recombination Kinetics in Photoconductors," Proceedings of the Third International Conference on Photoconductivity, p. 17-22, Pergamon Press, 1971.

17. Petritz, R. L. and Humphrey, J. N., "Photoconductivity of Lead Selenide: Theory of the Mechanism of Sensitization," Physical Review, v. 105, p. 1736-1740, 15 March 1957.

18. Klaassen, F. M., and others, "On the Temperature Dependence of the Photoconductive Decay Time of Films of the Lead Salts," Physics, v. 26, p. 623-628, August, 1960.

19. Hudson, R. D., Infrared Systems Engineering, Wiley, 1969.

20. Davidson, J. J., "Average vs RMS Meters for Measuring Noise," IRE Transactions on Audio, v. AU-9, p. 108-111, July, 1961.

21. Wolfe, W. L. ed., Handbook of Military Infrared Technology, U. S. Government Printing Office, 1971.

22. Jamieson, J. A., and others, Infrared Physics and Engineering, McGraw-Hill, 1963.

23. Holter, M. R., and others, Fundamentals of Infrared Technology, McMillan, 1962.

24. Kruse, D. W., McGlaughlin, L. D. and McQuistan, R. B., Elements of Infrared Technology, Wiley, 1962.

25. Potter, R. F. and Pernett, J. M., "The Measurement and Interpretation of Photodetector Parameters," Proceedings of the IRE, v. 47, p. 1503-1509, September, 1959.

26. Brower Laboratories, Inc., A Practical Guide to Measurement of Weak Signals Buried in Noise, 1968.

27. Princeton Applied Research, Instruction Manual: Lock-In Amplifier, Model 124, 1971.

28. Devillbiss, W. F. and Klunk, S. L., "Solid State Pulse Power Supplies in RCA GaAs Injector Lasers," RCA Optoelectronic Products Application Note An-4469, February, 1972.

29. Fisher, E., "Laser Diode Sub-Nanosecond Rise Time Source of Radiant Flux for Photodetection Testing," RCA Optoelectronic Products Application Note AN-4553, February, 1972.

30. Radio Corporation of America, Solid State Division, Solid-State Infrared-Emitting Diodes, Injection Lasers, Silicon Photodectors, (brochure), 1972.

31. Radio Corporation of America, Solid State Division, Gallium-Arsenide Lasers and Emitters, (brochure), 1972.

32. Kim, M. E., The Optical Properties and Energy Gap of Thin Lead-Tin Selenide Films in the Fundamental Absorption Edge Region, M.S. Thesis, University of California, Los Angeles, 1971.

33. Lowan, A. N. and Blanch, G., "Tables of Plank's Radiation and Photon Functions," Journal of the Optical Society of America, v. 30, p. 70-81, February, 1940.

34. Nill, K. W. and others, "Metal-Semiconductor Contacts on $Pb_{1-x}Sn_xTe$," The Physics of Semimetals and Narrow-Gap Semiconductors, p. 383-392, Pergamon Press, 1971.

35. Melngailis, I. and Harman, T. C., "Photoconductivity in Single-Crystal $Pb_{1-x}Sn_xTe$," Applied Physics Letters, v. 13, p. 180-183, September 1968.

36. Harman, T. C., "Narrow-Gap Semiconductor Lasers," Journal of Physics and Chemistry of Solids, v. 32, Supplement 1, p. 363, 1971.

37. Tao, T. F. and Wang. C. C., Narrow-Gap Semiconductors, U. S. Air Force Materials Laboratory Report AFML-TR-71-238 (unpublished), Wright Patterson Air Force Base, December, 1971.

INITIAL DISTRIBUTION LIST

		No. Copies
1.	Defense Documentation Center Cameron Station Alexandria, Virginia 22314	2
2.	Library, Code 0212 Naval Postgraduate School Monterey, California 93940	2
3.	Dr. T. F. Tao, Code 52 TV Department of Electrical Engineering Naval Postgraduate School Monterey, California 93940	5
4.	Professor A. Sheingold, Code 52 Sh Department of Electrical Engineering Naval Postgraduate School Monterey, California 93940	1
5.	LTJG Kurt E. Holmquist, USN 7011 Sea Cliff Rd. McLean, Virginia 22101	1
6.	CAPT W. G. McBride, USMC 808 Spring Dr. Mill Valley, California	1
7.	Dr. R. Morris (Code 421) Office of Naval Research Department of Navy Arlington, Virginia 22217	1
8.	Mr. R. Hickmott (AFML/LPE) Air Force Materials Laboratory Wright-Patterson Air Force Base, Ohio	1

Security Classification

DOCUMENT CONTROL DATA - R & D

(Security classification of title, body of abstract and indexing annotation must be entered when the overall report is classified)

ORIGINATING ACTIVITY (Corporate author)
Naval Postgraduate School
Monterey, California 93940

2a. REPORT SECURITY CLASSIFICATION
Unclassified

2b. GROUP

REPORT TITLE
Thin-Film $Pb_{0.9}Sn_{0.1}Se$ Photoconductive Infrared Detectors; Photoconductivity Measurements

DESCRIPTIVE NOTES (Type of report and inclusive dates)
Master's Thesis; December 1972

AUTHOR(S) (First name, middle initial, last name)
Kurt Ervin Holmquist

REPORT DATE	7a. TOTAL NO. OF PAGES	7b. NO. OF REFS
December 1972	129	37

CONTRACT OR GRANT NO.	9a. ORIGINATOR'S REPORT NUMBER(S)
PROJECT NO.	9b. OTHER REPORT NO(S) (Any other numbers that may be assigned this report)

DISTRIBUTION STATEMENT
Approved for public release; distribution unlimited.

SUPPLEMENTARY NOTES	12. SPONSORING MILITARY ACTIVITY
	Naval Postgraduate School Monterey, California 93940

ABSTRACT

$Pb_{0.9}Sn_{0.1}Se$ thin films were depositived on cleaved CaF_2 and BaF_2 substrates by vacuum evaporation methods. The as-deposited films were not photosensitive. Photo-conductivity was observed after the films had been isothermally annealed in Pb-Sn rich vapor to reduce their carrier concentrations. Blackbody (500° K) response measurements were made to determine the responsivity and detectivity of the thin-film samples. Blackbody responsivities as high as 60 volts per watt were measured. Thin films with single-crystal (100)-oriented structure were more sensitive than the films with either single-crystal (111) or polycrystalline mixed (111) and (100) structure. The wavelengths of photoconductive thresholds were determined by spectral response measurement and were in good agreement with the fundamental absorption edges. Photoconductive response times were measured using a GaAlAs heterojunction laser diode as the radiation source.

DD FORM 1 NOV 65 1473 (PAGE 1)
S/N 0101-807-6811

Security Classification

A-31408

KEY WORDS	LINK A		LINK B		LINK C	
	ROLE	WT	ROLE	WT	ROLE	WT
Thin-Film IV-VI Photoconductors